Communications Biology

https://doi.org/10.1038/s42003-026-09872-9

Article in Press

Polystyrene nanoplastics and benzo(a)pyrene synergistically induce lung fibrosis and inflammation via relaxin signalling in mice

Received: 11 July 2025

Accepted: 5 March 2026

Cite this article as: Chen, Y., Zhang, Y., Zhang, Y. *et al.* Polystyrene nanoplastics and benzo(a)pyrene synergistically induce lung fibrosis and inflammation via relaxin signalling in mice. *Commun Biol* (2026). https://doi.org/10.1038/s42003-026-09872-9

Yu Chen, Yingai Zhang, Yuting Zhang, Shuguo lv, Xu Zhang, Mohamed Mohsen, Xiaoshan Zhu, Kai Yin & Hailong Zhou

Polystyrene nanoplastics and benzo(a)pyrene synergistically induce lung fibrosis and inflammation via relaxin signalling in mice

Yu Chen[1], Yingai Zhang[2#], Yuting Zhang[3], Shuguo lv[4]， Xu Zhang[1], Mohamed Mohsen[5], Xiaoshan Zhu[6], Kai Yin[1]*, Hailong Zhou[1]*

1. School of Life and Health Sciences, Hainan Province Key Laboratory of One Health, Collaborative Innovation Center of Life and Health, Hainan University, Haikou, Hainan 570228, China.

2. Central Laboratory, Affiliated Haikou Hospital of Xiangya Medical College, Central South University, Haikou City Key Laboratory of Clinical Medicine, Haikou, Hainan, 570208, China

3. Shanxi Medical University, Taiyuan, Shanxi 030607, China.

4. Hainan Academy of Environmental Science, Hainan International Blue Carbon Research Center, Haikou 571126, China

5. Department of Fish Production, Faculty of Agriculture, Al-Azhar University, Nasr City, Cairo, 11884, Egypt

6. School of Ecology, Hainan University, Haikou, Hainan 570228, China.

Co-first author

* To whom correspondence should be addressed:

Kai Yin

School of Life and Health Sciences, Hainan University, Haikou; 570228, China.

996523@hainanu.edu.cn

Hailong Zhou

School of Life and Health Sciences, Hainan University, Haikou; 570228, China.

zhouhl@hainanu.edu.cn

Abstract

Micro- and nanoplastics (MNPs) are emerging pollutants that can carry harmful substances like benzo(a)pyrene, posing potential health risks. While the harmful effects of nanoplastics on the lungs are known, how they interact with benzo(a)pyrene to affect cellular communication remains unclear. In our study, We explore this interplay using a 16-week mouse model exposed to environmentally relevant doses of polystyrene nanoplastics, benzo(a)pyrene, or a combination of both. We find that only the combined exposure leads to significant lung damage, characterized by severe inflammation and tissue scarring, which are not seen with single exposures. This combined exposure also increases oxidative stress and reduces antioxidant defenses in the lungs. Furthermore, we notice increased levels of inflammation-related molecules and markers of lung tissue damage, confirming a more severe toxic effect. Transcriptomic analysis highlights the involvement of the Relaxin signaling pathway, which influences inflammatory and tissue damage processes through PI3K-AKT and MAPK cascades; Relaxin4 activated PLC-IP3R, opening ER calcium channels and raising cytosolic Ca^{2+}, which triggered macrophage extracellular trap (MET) formation. Additionally, a macrophage-MLE-12 co-culture system confirmed that Mix-induced METs are linked to the exacerbation of alveolar inflammation and the progression of pulmonary fibrosis. Our findings reveal novel molecular connections that explain how these pollutants worsen lung health, suggesting that targeting the identified signaling pathways could offer a potential approach to mitigating these harmful effects.

Keywords: polystyrene nanoplastics (PS-NPs); benzo(a)pyrene (BaP); Relaxin signaling; macrophage extracellular traps (METs); lung fibrosis; inflammatory response

Introduction

Global plastic production has grown exponentially (from 2 million tonnes in 1950 to 348 million tonnes in 2017) and is expected to reach 1.2 billion tonnes in 2050 [1]. This large-scale production and use have led to the accumulation of plastic waste in the environment, which gradually degrades into microplastics (MPs; <5 mm in diameter) and nanoplastics (NPs; <100 nm in diameter) through processes such as photo-degradation, thermal oxidation, and mechanical abrasion[2, 3]. Due to their tiny particle size, wide distribution, and persistence, MPs and NPs have been detected in water, soil, and atmosphere. These particles can enter the human body via the food chain, drinking water, and inhalation [4, 5]. Particle tracking analysis of polystyrene (PS) has shown that it takes about 56 days to form nanoplastic particles (NPs) [6, 7]. Studies on zebrafish embryos have reported that NPs exposure can impair hatching and survival rates and inhibit embryonic growth[8]. Moreover, MPs and NPs have been detected in the human body [9-11], such as in the lungs, liver, blood, intestines, and spleen, suggesting their systematic bioaccumulation and potential health risks [12-14]. Furthermore, NPs can penetrate the intestinal and alveolar barriers and accumulate in cardiac tissues, which induce pathological changes such as arrhythmia, pericardial effusion, and myocardial fibrosis [13]. A wide range of plastic particles have been observed in lung tissue by infrared spectroscopy, where their exposure can trigger oxidative stress, inflammatory response, and cellular translocation [15-17]. Although the environmental behavior and ecotoxicity of MNPs have attracted widespread attention, their long-term effects on human health, especially the potential hazards to the respiratory system, remain poorly understood and demand further investigation.

MNPs also act as vectors for other pollutants, especially typical persistent organic pollutants (POPs), such as Polycyclic aromatic hydrocarbons (PAHs) [18]. Their unique physicochemical properties [19, 20] and high hydrophobicity enhance their ability to adsorb and transport such pollutants [21]. Consequently, MNPs often act as carriers to translocate pollutants to organisms[22]. Benzo(a)pyrene (BaP), a typical representative substance of PAHs, has significant teratogenicity and carcinogenicity[23]. BaP induces DNA damage, mitochondrial dysfunction, oxidative stress, and other mechanisms that lead to cellular damage [24]. Also, BaP is able to promote Ca^{2+}-dependent lysophosphatidylcholine (LPC) production by modulating phospholipase A2 activity in alveolar cells, thus triggering lung tissue injury [25].

As the core organ of the human respiratory system, the lungs maintain key physiological functions such as gas exchange, immune defense, and metabolic homeostasis. Studies have shown that MNPs can disrupt lung homeostasis through multiple pathways, including the generation of reactive oxygen species (ROS), leading to an imbalance in the oxidative-antioxidant system. Also, they induce the overexpression of pro-inflammatory factors through the modulation of key signaling pathways, such as NF-κB. Furthermore, they interfere with the process of cellular autophagy, affecting the clearance of damaged organelles [15, 26, 27]. For instance, PS-NPs significantly elevate ROS levels in lung epithelial cells, leading to decreased mitochondrial membrane potential and DNA damage, triggering programmed death pathways such as apoptosis and necrotic apoptosis[28, 29]. Similarly, BaP exposure alters fatty acid synthesis, suppresses immunity, and induces oxidative stress, contributing to acute lung injury [30].

Pulmonary fibrosis is a progressive pathological change manifested by abnormal

accumulation and remodeling of collagen and extracellular matrix (ECM) [31]. Macrophages, as important immune cells in lung tissues, perform a variety of functions in the lung, including immune defense, inflammation regulation, tissue repair, and fibrosis regulation[32].. Exposure to MPs activates a variety of immune cells (e.g., lymphocytes, macrophages, and NK cells), promotes the release of inflammatory factors (TNF-α, IL-6, IL-8, etc.), and creates a pro-inflammatory microenvironment [33, 34]. BaP exposure significantly up-regulates the expression of inflammatory markers in the larval model and promotes neutrophil recruitment to the site of injury, as well as inducing skeletal deformities in zebrafish[35, 36]. Macrohages extracellular traps (METs) are networks of DNA, histones, and antimicrobial proteins released by macrophages to defend against pathogen invasions[37]. Excessive METs act as inflammatory mediators inducing a hyperinflammatory signaling cascade response leading to tissue damage and inflammation. Macrophages release METs in a ROS-dependent manner, and cells crosstalk with each other to produce pro-inflammatory effects from induced extracellular traps[38]. METs can promote liver injury through the classical fibrotic ROS/TGF-β/Smad2/3 signaling axis[39]. Studies of cellular entrapment networks (ETs) mediating tissue injury under the stimulation of specific NPs and BaP are still unknown. The current mechanism of action of METs on lung injury still needs to be further explored.

It has been shown that the binding of MPs to BaP may have cumulative, synergistic, or antagonistic effects[40]. MPs enhance the bioaccumulation and toxic effects of BaP in aquatic organisms by forming a complex pollutant [41]. These pollutants act synergistically to promote senescence through damage to mitochondria of *Cryptococcus showyi* nematodes and disruption of

oxidative homeostasis in vivo [42]. In earthworm cells, PS-NPs and BaP synergistically induced oxidative stress with a significant elevation of ROS levels under combined exposure by affecting the structure of Tyr 357, the active center of CAT enzyme, they inhibit H_2O_2 catabolism and exacerbate oxidative damage [24]. This synergistic effect has been demonstrated in invertebrate models, but the toxic effects in mammals remain to be investigated.

Relaxin, a peptide hormone initially linked to the reproductive system during pregnancy, has since been found to participate in various physiological and pathological processes [43]. The dual role of the Relaxin signaling pathway in the fibrotic process provides a new perspective for [44]understanding pollutant-induced lung injury. While relaxin is widely recognized for its antifibrotic effects via inhibition of TGFβ1/Smad3 signaling[45] , emerging evidence indicates that its role in fibrosis is highly context-dependent. In acute injury models, relaxin activates Gαs-cAMP/PKA pathways to suppress fibrosis [46, 47]. However, under chronic oxidative stress or environmental pollutant exposure, RXFP1 may undergo G protein switching or receptor desensitization[48] [49], diverting signaling toward PI3K-AKT and MAPK cascades that promote fibroblast activation and ECM deposition [50, 51] . This functional plasticity suggests that relaxin signaling can be reprogrammed from anti-fibrotic to pro-fibrotic depending on the specific pathological microenvironment[52].Upregulation of the RXFP1 signaling pathway has been reported to promote endothelial-mesenchymal transition (EndMT) and induce injury under certain pathological conditions [53]. Relaxin may exacerbate the fibrotic process by promoting ECM deposition through activation of the PI3K-AKT and MAPK signaling pathways [54-56]. However, the mechanism of relaxin-induced pulmonary fibrosis remains inconclusive.

Most previous studies have focused on acute or high-dose exposures to NPs and BaP, while the chronic effects of environmentally relevant, low-dose exposures on lung health remain largely unknown. The synergistic effects of these pollutants in inducing pulmonary fibrosis also remain to be elucidated. In this study, we developed mouse models of exposure to environmental concentrations of PS-NPs and BaP alone and in combination, an exposure condition that is more consistent with real-life scenarios of human life. We attempted to characterize the release of macrophage METs to investigate the possibility of METs inducing lung injury and to determine the mechanisms of the relaxin signaling pathway in regulating lung fibrosis. A potential scientific explanation for the chronic health risks triggered by the combined toxic effects of NPs-carried BaP is provided.

Results

PS-NPs and BaP co-exposure induces lung inflammation and fibrosis

During the animal model construction process, the body weight and organ weights of the mice were recorded every two weeks. As shown in Figure 1A, there was a significant increase in body weight in the Mix exposure group between 6 weeks and 10 ($p < 0.001$), The organ coefficient of mouse lung tissue showed an increasing trend in the PS-NPs exposure group at week 4 ($p = 0.005$); meanwhile, the mixed exposure group only showed a slight increase at week 8 ($p = 0.01$). The results showed that long-term exposure at low concentrations caused mild effects on the body weight and organ coefficient of mice due to chronic toxicity(The same data presented in two formats) (Figure 1B and Supplementary figure 1).

The results of the histological evaluation showed that the lung tissue structure of the control group (Con) was normal, with no significant pathological changes; the Mix group presented significant tissue damage, characterized by local alveolar structure atrophy with thickening of the alveolar septa (black arrows), noticeable shedding of bronchial epithelial cells (yellow arrows), accumulation of foam cells (green arrows), and a large number of inflammatory cells infiltration (red arrows) (Figure 1 C), with the damage in the BaP and PS-NP groups being less severe.

Furthermore, the protein levels of inflammation-related indicators IL-1β ($P = 0.0001$) and TNF-α ($p = 0.0006$) were significantly higher than those in the Con group (Figure 1E and F). Moreover, indicators related to oxidative stress in lung tissue were detected (Figure 1D). The data showed a significant decrease in antioxidant indicators (GSH/GSSG, CAT, T-AOC, SOD) ($p <$

0.001), and a significant increase in oxidative damage indicators (MDA) ($p < 0.001$), indicating that the treatments disrupted the antioxidant levels of lung tissue, causing oxidative stress. Inflammation and oxidative stress, as key drivers of the fibrotic process, interact through a complex signaling network, synergistically promoting the occurrence and progression of fibrosis. The degree of lung tissue fibrosis was assessed using Masson's trichrome staining method. The results showed. (Figure 1G). Combined with the analysis of protein expression related to lung tissue fibrosis, the upregulation of S100A9 ($p < 0.0001$) induced the expression of α-SMA ($p = 0.01$) and Collagen ($P=0.0004$) proteins, showing an upward trend compared to the control group (Figure 1H). HYP levels were significantly elevated in all experimental groups, with the highest levels observed in the MIX group, indicating the most pronounced collagen deposition (Figure 1I).Overall, suggest that the observed pulmonary effects are associated with the test substance rather than the operational process, FTIR reveals π-π stacking of BaP onto PS-NPs, prolonging retention and C=O-driven ROS to amplify inflammation and fibrosis(Supplementary figure 2).these results suggest that combined exposure to PS-NPs and BaP can induce inflammatory and fibrotic damage in lung tissue.

PS-NPs and BaP co-exposure induce the production of METs

To further investigate the mechanism observed in vivo, in vitro experiments were performed using the RAW264.7 macrophage cell line (Figures 2A–B). First, cells were exposed to a range of concentrations of PS-NPs and BaP. Exposure to 100 μg/ml of either compound did not reduce cell viability. However, exposure to PS-NPs at 200 μg/ml and BaP at 300 μg/ml and above reduced the viability of macrophages (RAW264.7). Therefore, concentrations of 100 μg/ml PS-NPs, 100 μg/ml

BaP, and a mixture of 100 μg/ml PS-NPs + 100 μg/ml BaP were chosen for subsequent experiments. Hochest staining showed that exposure to BaP, PS-NPs, and the mixed group induced the formation of DNA-skeleton reticular structures in macrophages, with the mixed group showing the most reticular structures. The positive control (LPS) further enhanced the formation of these structures (Figure 2 C).

Furthermore, the DCFH-DA fluorescent probe was used to detect the level of intracellular reactive oxygen species (ROS), and the results showed that the fluorescence intensity of RAW264.7 cells increased in a dose-dependent manner with exposure concentration. The fluorescence intensity of the mixed group was the highest ($p < 0.001$). This indicates that under exposure to pollutants, the mixed group had the most significant stimulation of macrophages, causing oxidative stress in the cells (Figure 2 D). Immunofluorescence results showed that Cith3 ($p = 0.005$) and MPO ($p = 0.02$) proteins were highly expressed in the network structures induced by the mixed group, indicating that these structures are METs. Therefore, the mixed group was selected for subsequent mechanistic investigations (Figure 2E).

METs mediate lung inflammation and fibrosis

To determine whether METs contribute to the lung inflammation and fibrosis induced by PS-NPs and BaP, an in vitro co-culture model was established using mouse lung epithelial cells (MLE-12) and macrophages (RAW264.7) (Figure 3A). RAW264.7 cells were added to the MLE-12 cells and then treated with the combined PS-MPs + BaP exposure to induce the production of METs. Assessment of cellular ROS levels revealed that the combined group treatment exhibited

significantly higher oxidative stress ($p < 0.001$) than that of MLE-12 cells and RAW264.7 cells alone (Figure 3B). Under the combined exposure, METs in the co-culture system were detected, and Cith3 (Figure 3C) and MMP9 (Supplementary figure 3B) proteins were detected by immunofluorescence in the co-culture cell group. Meanwhile, the MLE-12 cell group produced inflammatory factors IL1β (Supplementary figure 3 A). However, the expression of IL-1βproteins in the co-cultured RAW264.7 cells was significantly increased ($p < 0.001$), indicating that METs amplify the inflammatory response. Notably, this increase could be reversed by Dnase I , demonstrating the functional role of extracellular DNA scaffolds in mediating inflammation. In addition, immunofluorescence (IF) results showed that, compared with the MLE-12 Mix group, the levels of fibrotic collagen I and TGF-β in the co-culture exposure group were significantly increased, similar to the positive control ($p < 0.001$) (Figure 3D). Collectively, these results suggest that the production of METs plays an important mediating role in inducing inflammation and fibrosis in lung tissue.

PS-NPs and BaP co-exposure activates the Relaxin signaling pathway

To further dissect the molecular mechanisms underlying lung injury induced by PS-NPs and BaP co-exposure, we performed transcriptomic analysis (Supplementary figure 4).To explore mechanisms of PS-NPs plus BaP lung injury, Venn analysis of DEGs revealed 12,090 co-expressed genes across CON, BaP, PS and MIX, forming a common transcriptional backbone. Treatment-specific signatures were small—138, 223 and 89—indicating limited unique responses, useful for targeted validation. Gene ontology (GO) enrichment analysis on the differentially expressed genes indicated that the biological processes were mainly enriched in

immune-related processes (Figure 4B). This is consistent with the central role of macrophages as a core component of the immune system, playing a significant role in both innate and adaptive immunity. Subsequently, a KEGG enrichment analysis of the differentially expressed genes in lung tissue was conducted. The results revealed that the differentially expressed genes between the control group and the combined group were enriched in the Relaxin signaling pathway (Figure 4C), with qRT-PCR and Western blotting detection results showing consistent outcomes . All primer sequences used for qPCR are listed in table 1, the expression of RXFP1, RXFP3, and RXFP4 at both mRNA and protein levels was significantly increased ($p < 0.001$) at PS-MPs group, BaP group, and Mix group, with the expression level in the Mix group exhibitibg the most significant effect (Figures 4D, F). In summary, these results suggest that the Relaxin signaling pathway in lung tissue is activated during the Mix exposure period, suggesting its potential involvement in the development of inflammation and fibrosis.

Relaxin 4 signaling pathway promotes METs formation through endoplasmic reticulum calcium release

As shown in Figures 4D and E, the Relaxin 4 pathway is activated in the Mix exposure group. Therefore, we further examined the activation of PLC-IP3R in lung tissue. Compared with the Con group, the expression levels of IP3R and PLC proteins in the Mix group were significantly increased ($p < 0.001$) (Figure 5B). To assess changes in intracellular calcium dynamics, immunofluorescence staining was performed (Figure 5A). PMA (Phorbol 12-myristate 13-acetate, 100 nM, 4 hours) is often used as a positive control for maximal ROS generation and NET/MET formation[61]. After stimulation with the positive inducer PMA, the amount of calcium ion

generation significantly increased (P=0.01), and the endoplasmic reticulum calcium ion content in the Mix group was higher than that in the Con group ($p = 0.003$). Consistent with calcium signaling activation, the protein expression levels of METs-related markers MPO and Cith3 in the lung tissue of the Mix group were significantly upregulated compared to the control ($p < 0.001$) (Figures 5C and 5D). The experimental results indicate that the Mix exposure activates PLC-IP3R through Relaxin to release calcium ions, and the release of calcium ions promotes the formation of METs.

Furthermore, the expression of MMP9 protein, a protein associated with both METosis and fibrosis, was significantly elevated ($p < 0.001$), inducing the occurrence of fibrosis by the production of METs. To further validate the role of calcium signaling, a calcium ion chelator was added to block the generation of calcium ions. It can be seen that the amount of calcium ion generation in the Nifedipine group was significantly reduced (Figure 5E). Compared with the control group, the expression level of IP3R protein in the Mix group was decreased ($p = 0.003$), and the activity of PLC was almost unaffected (Figure 5F). Overall, the expression levels of related METs and fibrosis proteins in mouse lung tissue were upregulated, and the release of calcium ions through the calcium ion channel was verified at the in vitro cell level. This indicates that endoplasmic reticulum calcium ions can mediate the formation of METs to promote the occurrence of fibrosis, and the method of inducing METs release by calcium ions can be alleviated by chelators.It is noteworthy that the effect disappeared after nifedipine treatment, suggesting that this process is calcium-dependent. However, this study failed to distinguish the specific source of calcium ions. Future studies should use specific endoplasmic reticulum calcium channel inhibitors (such as xestospongin C or dantrolene) to further verify the role of endoplasmic reticulum calcium

release.

Relaxin 1 and Relaxin 3 signaling pathways regulate inflammation and fibrosis through PI3K-AKT, MAPK

Evidence showed that Relaxin 1 and Relaxin 3 in the Relaxin signaling pathway were activated under the Mix exposure group (Figure 4D). Western blot analysis revealed that the phosphorylation level of P38 in the Mix group was significantly increased ($p < 0.001$), and the phosphorylation levels of JNK ($p = 0.002$) and ERK ($p = 0.01$) were also upregulated compared to the control (Figure 6A). These protein-level findings were consistent with qRT-PCR results, which showed significantly increased mRNA expression of P38, ERK, and JNK ($p < 0.001$), verifying that the MAPK pathway was activated. The role of phosphorylated p38 MAPK (phosphorylation at Thr180/Tyr182) in fibrotic progression was further supported by its association with the upregulation of α-SMA expression (Supplementary figure 5 B) and increasing collagen I secretion (Figure 1G and 3D).

As shown in Figure 6B, the total phosphorylation levels of PI3K ($p = 0.02$) and AKT ($p = 0.009$) in the Mix group increased by about 50% compared to the control group. Additionally, the phosphorylation protein expression level of I-κB was significantly increased ($p = 0.01$). The mRNA expression levels of PI3K ($p < 0.001$) and AKT ($p = 0.003$) were significantly elevated, confirming that the PI3K-AKT and NF-κB signaling pathways had been activated (Figure 6C). Also, qRT-PCR detection further confirmed that the mRNA expression of pro-inflammatory factors (TNF-α and IL-1β) in the lung tissue of the Mix group significantly increased ($p < 0.001$)

(Figure 6D). The activation of the NF-κB signal and the PI3K-AKT signaling pathway was linked to the regulation of MMP9 protein. Furthermore, immunofluorescence staining results of lung epithelial cells (MLE-12) showed that the relative fluorescence intensity of fibrogenesis-related markers MMP9 and α-SMA significantly increased compared with the control group ($p < 0.001$) (Supplementary figure 5B). Additionally, the expression of E-cadherin decreased ($p = 0.02$) (Figure 6E), indicating EMT deposition and myofibroblast activation, associated with fibrosis progression. In summary, co-exposure to PS-NPs and BaP activates Relaxin 1 and Relaxin 3 signaling, which in turn, initiates PI3K-AKT and MAPK pathways. These cascades may contribute to the inflammatory response and fibrosis through the induction of EMT, immune cell recruitment, and ECM remodeling.

Discussion

PS-NPs and BaP are ubiquitous environmental, and their combined exposure poses risks to respiratory health due to synergistic toxicity. PS-NPs can act as carriers[62], adsorbing BaP and facilitating its accumulation in lung tissue, thereby intensifying oxidative stress and inflammatory responses[63]. This phenomenon is often referred to as the "Trojan horse", which may be an important mechanism of synergistic toxicity[21]. However, the comprehensive impact of PS-NPs and BaP under environmentally relevant concentrations is not fully understood, especially regarding their interaction with immune cells in the lungs. Here, we exposed mice to BaP and PS-NPs, both individually and in combination, for a 16-week period. The results showed that the combined exposure to BaP and NPs was associated with inflammatory responses, METs release, and activation of the Relaxin pathway, which may contribute to lung fibrosis damage.

Upon exposure to external stimuli (such as pathogens, pollutants, or injuries), macrophages play a crucial role in the lungs[64]. To counter external stimuli, the mucous layer and cilia of the lungs work together to capture and clear foreign particles, including PS-NPs and BaP, from the respiratory tract. NPs and BaP activate alveolar macrophages and epithelial cells, releasing inflammatory factors[65]. These inflammatory factors recruit inflammatory cells, such as neutrophils and macrophages, to the site of injury, exacerbating the inflammatory response. Macrophages not only serve as the first line of defense in immune defense but are also key cells in regulating inflammatory responses, tissue repair, and fibrosis[66, 67]. Macrophages release a mesh-like structure with DNA as the backbone (METs) when stimulated by external factors, which is similar to NETs and was initially discovered by Brinkmann et al. [61, 68]. METs can be released

upon stimulation by various pro-inflammatory factors and are capable of capturing and clearing pathogens. In this study, we found that both PS-NPs and BaP, alone and in combination, resulted in the formation of network structures, with the greatest increase increase in METs observed in the combined exposure group. While METs are part of the innate immune response, their excessive release can also lead to fibrotic damage[69]. We used immunofluorescence to detect the upregulation of MPO and Cith3, confirming the release of METs, as well as the significant increases in inflammatory markers such as IL-1β and TNF-α, and fibrotic markers like α-SMA [39].

The formation mechanism of METs includes both ROS-dependent and independent pathways. In the ROS-dependent pathway, external stimuli-induced respiratory burst that promotes the massive production of METs, which induces hepatitis[38]. Studies have shown that diphenyleneiodonium (DPI) treatment did not significantly inhibit the release of METs from goat monocyte-derived macrophages[66]. In the ROS-independent pathway, such as the Relaxin4 signaling pathway, MET formation is triggered by intracellular calcium release from the endoplasmic reticulum. Mechanistically, PLC catalyzes the hydrolysis of PIP2 to produce DAG and IP3R, both of which act as second messengers to regulate cellular processes. DAG remains on the membrane, while IP3R is released into the cytoplasm and diffuses to the endoplasmic reticulum, binding to IP3R receptors (IP3R) to activate calcium channels, resulting in an increase in cytoplasmic calcium concentration[70]. During the formation of METs, the cytoplasmic Ca^{2+} concentration increases, activating peptidylarginine deiminase 4 (PAD4), which catalyzes histone citrullination, thereby inducing chromatin decondensation. The application of calcium chelators effectively suppressed calcium release and significantly reduced MET structures, These findings

confirm the pivotal role of calcium signaling in MET induction. Our results demonstrate that the combined exposure group activates the PLC-IP3R pathway via Relaxin, facilitating calcium ion release and thereby regulating MET formation. This was further supported by inhibition experiments using calcium chelators. METs can act as inflammatory mediators, functioning in other cells. For example, METs released by macrophages exacerbated oxidative stress and liver ischemia/reperfusion (I/R) injury in AML12 hepatocytes [71]. Similarly, MET-induced inflammation has been implicated in brain endothelial dysfunction [72]. In this study, the co-culture of RAW264.7 macrophages with MLE-12 lung epithelial cells revealed that METs induced by PS-NPs and BaP upregulated inflammatory and EMT-related genes, which verified the damage mediated by METs. Under the stimulation of PS-NPs and BaP, upregulation of pro-inflammatory responses and genes related to pro-EMT in co-cultured RAW264.7 and MLE-12 lung cells was observed through IF, and this cascade of reactions was reduced by DNase I. These results suggest that METs may play a key role in lung fibrosis induced by environmental pollutants.

Studies have shown that the invasion of exogenous substances leads to oxidative stress, and excessive production of ROS is considered one of the factors causing damage to organisms [73]. PS-MPs can induce the formation of ROS in BEAS-2B cells, causing cytotoxicity and inflammatory effects, disrupting the lung barrier, and triggering lung diseases[73]. Further, Jong et al. found that mitochondrial damage is mediated through the production of ROS and the infiltration of inflammatory cells, inducing lung inflammation through the NF-κB pathway[74]. In this study, mice exposed to PS-NPs and BaP exhibited significant alterations of oxidative stress markers, such as T-AOC, SOD, MDA, etc., through the detection of antioxidant enzymes and oxidative damage,

triggering oxidative stress and promoting inflammatory responses. Inflammatory cells (such as macrophages, neutrophils) produce a large amount of ROS through respiratory bursts, further aggravating oxidative stress[75]. At the cellular level, the increase in oxidative stress and inflammation levels may directly affect the degree of fibrosis levels. ROS is associated with activation of NF-κB and MAPK signaling pathways and inflammatory factor expression and the infiltration of inflammatory cells[76]. Furthermore, specific regulators such as FOXM1 and MKP1 have been implicated in fibrosis through modulation of these pathways. For instance, the deletion of FOXM1 (myFoxm1-/-) in macrophages. FOXM1 inactivation promotes lung injury by inhibiting DUSP1 expression and activating p38 MAPK signaling[77]. Also, MKP1 promotes the dedifferentiation of lung myofibroblasts and restores apoptosis sensitivity through dephosphorylation of p38α MAPK, and the specific deletion of MKP1 in fibroblasts inhibits the regression of bleomycin-induced fibrosis[78]. Similar results were obtained by qRT-PCR and Western blotting determinations in this study, with NPs and BaP exposure enhancing the phosphorylation levels of NF-κB and MAPK, further promoting the upregulation of IL-1β, TNF-α, which has been confirmed to regulate the classical regulatory pathway of inflammation[79].

This study found that co-exposure to PS-NPs and BaP can significantly activate the relaxin signaling pathway, although the direct role of relaxin in promoting fibrosis remains to be studied. Our data suggest that Relaxin1 may promote fibrotic signaling through MAPK activation., Specifically, phosphorylation of p38 MAPK (Thr180/Tyr182) increased α-SMA expression and collagen I secretion, promoting pulmonary fibrosis. The PI3K-AKT pathway also appears to play a central role in Relaxin-mediated effects, which is closely related to the RXFP3 pathway. Studies

by Qi et al. have shown that TUG1 knockout suppresses inflammation, EMT, activates autophagy, and blocks the expression of the PI3K/Akt pathway, alleviating pulmonary fibrosis[55, 80]. Additionally, LPS promotes the synthesis of collagen in lung fibroblasts by upregulating the expression of proteins in this pathway through aerobic glycolysis[56]. Mechanistically, PI3K catalyzes the conversion of PIP2 to PIP3R, recruiting AKT to the cell membrane and phosphorylating it for activation. The activated PI3K-AKT pathway promotes the degradation of IκBα and the nuclear translocation of NF-κB. Subsequently, NF-κB upregulates the expression of inflammatory factors (such as TNF-α, IL-6, IL-1β), worsening the inflammatory response.

There is also a relatively complex interaction between PI3K-AKT and MAPK, which together regulate the process of fibrosis[81]. Our results showed that the protein levels of Relaxin4 pathway-related proteins PLC and IP3R are upregulated, which is associated with increased calcium ion content and extracellular trap release, factors that may contribute to lung injury. Collectively, the Relaxin signaling pathway, through the activation of Relaxin1, Relaxin3, and Relaxin4, the upregulation of the MAPK and PI3K-AKT phosphorylation signaling network, and the increase in calcium ion content, promotes the expression of downstream MMP9 protein and the release of METs. Furthermore, the downregulation of E-cadherin indicates the loss of adhesion properties of epithelial cells and the upregulation of α-SMA, indicating the synthesis of the extracellular matrix, thereby promoting the activation of fibroblasts and abnormal deposition of ECM .Although hydroxyproline quantification was not performed, Masson staining, α-SMA/Col1a1 expression, and immunofluorescence results consistently show a significant increase in collagen deposition, sufficient to support the diagnosis of fibrosis. In future studies,

hydroxyproline measurement will be supplemented in new batches of samples for further absolute quantification. Thus, we elucidated the relationship between the Relaxin signaling pathway and METs. Elaxin4 may be associated with PLCγ activation via the AKT-mTORC1 axis pathway, which may contribute to IP3R generation and calcium release from the endoplasmic reticulum, factors associated with MET production. Meanwhile, p38 MAPK can activate the NOX2 complex, promoting the burst of ROS, which can activate histone citrullination mediated by PAD4, promoting chromatin decondensation and the release of METs. METs further aggravate lung injury[82]. Our study uncovers a novel mechanistic link between the Relaxin signaling pathway and METs in promoting pulmonary fibrosis, highlighting their potential as targets for future investigations. Consistent with recent studies [83-85], our IP3R--PLC inhibition experiment demonstrates that Relaxin1/3→PI3K-AKT/MAPK and Relaxin4→PLC-IP3R-Ca^{2+}→METs operate in parallel, jointly amplifying lung inflammation and subsequent fibrosis [86, 87].

This study used intratracheal instillation to simulate respiratory exposure. Although this method cannot replicate the dynamics of natural human inhalation exposure (such as intermittency and concentration fluctuations), it is a commonly used approach for simulating cumulative respiratory exposure to micro- and nanoplastics [83]. The '10 years of human exposure' mentioned in the study was calculated using an 'environmental concentration–respiratory volume–cumulative equivalence' model: based on micro- and nanoplastic concentrations in the air, combined with the daily adult respiratory volume (approximately 11.3 m^3/day) to convert to daily exposure, the total exposure over 10 years was then converted to a mouse dosing regimen using the OECD body weight adjustment formula [86]. However, in real environmental conditions, the continuity and

concentration variability of human exposure differ from the experimental model [84], and subsequent inhalation exposure experiments are needed to verify the real-world environmental significance of this dosage.

In summary, this study reveals a novel association between chronic co-exposure to PS-NPs and BaP and pulmonary fibrosis, mediated through the Relaxin signaling pathway. Our findings demonstrate that combined exposure activates Relaxin signaling via dual mechanisms: Relaxin1/3-mediated PI3K-AKT/MAPK activation correlates with increased inflammation and ECM deposition, while Relaxin4-dependent PLC-IP3R signaling is linked to elevated ER calcium levels and MET formation. These parallel cascades appear to contribute to the amplification of lung inflammation and fibrotic progression, suggesting environment-dependent plasticity of relaxin signaling under chronic pollutant exposure. This work elucidates molecular circuits linking environmentally relevant nanoplastic-PAH co-exposure to pulmonary fibrosis and identifies the Relaxin-Ca^{2+}-MET axis as a potential candidate for further investigation as an intervention target.

Methods

Preparation of the Polystyrene Nanoplastics and Benzo[a]pyrene

Polystyrene NPs (PS-NPs, 2.5% w/v, 10 mL; 100 nm diameter) were purchased from Tianjin Besler Chromatography Technology Development Centre and BaP was obtained from Sigma Company.

Animals and experimental design

Five-week-old male Kunming mice (20 ± 2 g) were purchased from Guangdong Laboratory

Animal Centre (Guangzhou, China) and acclimatized for 7 days. Mice were randomly assigned to four groups (n = 40 per group, 5 per cage): (1) Control group (treated with pure water), (2) PS-NPs group (1 mg/kg), (3) BaP group (252 μg/kg), and (4) PS-NPs + BaP combined exposure group (Mix group). All substances were administered via airway intubation and sonicated for 30 min before each day's administration to ensure uniform dispersion of PS in water. Intratracheal instillation was performed every 72 hours for 16 weeks (a total of 37 times)[57]. Each dose contained 12 μg of PS-NPs and 0.3 μg of BaP, dissolved in 50 μL of saline. The cumulative lung burden corresponds to the upper-end exposure level of humans over 10 years in heavily polluted cities (PM2.5 concentration 150 $\mu g/m^3$; BaP concentration 15 ng/m^3)[58-60]. During the experiment, behavioral observations, respiratory function, appearance of feces, and environmental monitoring were conducted at different frequencies（Supplementary table 1）. Humane endpoints were set according to national standards and AAALAC guidelines. All data were double-checked by two people and backed up twice in Excel for traceable verification. After 16 weeks of exposure, Mice were deeply anesthetized with isoflurane (5% in O_2) and blood was collected via cardiac puncture, followed by immediate collection of lung tissue for histological and molecular analysis . Lung tissues were collected and either fixed in 4% paraformaldehyde (PFA) or stored in liquid nitrogen for backup. All experimental procedures were approved by the Animal Care Committee of Haikou People's Hospital, approval number: SC20230241.

Hematoxylin and eosin (H&E) staining

Lung tissues were fixed in 4% paraformaldehyde solution and prepared into wax blocks.

The wax blocks were cut into 5 μm thick sections using a slicer, dewaxed and washed, and stained with hematoxylin and eosin (HE)(Beyotime, C0105S). Finally, sections were observed under a light microscope.

Collagen fiber staining

Tissue samples were sectioned after paraffin embedding, fixed in 4% paraformaldehyde for 10-15 minutes, and rinsed in PBS. The samples were dehydrated sequentially with different concentration gradients of ethanol for 2-3 min. per step. After xylene treatment for transparency for 5 min., samples were stained with drops of Masson's stain (G1340, Solarbio) for 10-15 min. PBS or distilled water was used to wash away the residual stain, dehydrating again with ethanol, xylene transparency, and finally sealing the slices with neutral gum, to the light microscope for observation of the collected images.

Transcriptomic analysis

After 16 weeks of exposure to airway intubation, lung tissues from each group were subjected to transcriptome sequencing. First, RNA was extracted using the Trizol method, purified, quantified, and subjected to transcriptome sequencing (Beijing Novogene Technology Co., Ltd). Gene function annotation was performed using 7 databases (e.g., NR, SwissProt, KOG, etc.) with tools such as Blast2GO and HMMER, using E-value thresholds set at 1e-5 to 1e-6, to ensure the accuracy of the data.

Antioxidant biochemical assay

According to a weight (g) to volume (mL) ratio of 1:9, add nine times the volume of saline,

prepare a 10% homogenate under ice-water bath conditions, centrifuge at 2500 rpm for 10 minutes, and collect the supernatant for testing. Commercial kits were used to assess Glutathione (GSH), total antioxidant capacity (T-AOC), total superoxide dismutase (T-SOD), malondialdehyde (MDA), and catalase (CAT) activities (Nanjing Jiancheng Bioengineering Institute).

Culture and passage of macrophages culture

RAW264.7 (ATCC TIB-71) and MLE-12 (ATCC CRL-2110) were both purchased from ATCC and have undergone STR authentication and mycoplasma testing. Cell were cultured in high-glucose DMEM medium containing 10% fetal bovine serum and 1% penicillin-streptomycin (Biosharp) in an incubator at 37.5°C, 5% CO2, and passaging was performed every 2 days.

Cell viability assay(cck8)

Macrophages were inoculated for 24 h and treated with different concentrations of PS-NPs (0, 25, 50, 100, 200, 300, 400 μg/ml) or BaP (0, 25, 50, 100, 300, 500, 700 μg/ml). Thereafter, cells were washed with PBS 3 times, and CCK-8 reagent (DOJINDO) was added. The cells were incubated for 2 hours and cell viability was measured using an enzyme marker.

METosis formation observation

Macrophages were inoculated for 24 h and treated with different concentrations of PS-NPs and BaP. Lipopolysaccharide (LPS, Solarbio; 0.5 μg/ml) was used as a positive inducer of METs. After treatment, cells were washed three times with PBS, stained for 30 min by adding 5 μg/ml Hoechst 33258 (Solarbio), washed with PBS, and observed under a microscope. DNase I (Solarbio; 5 mg/ml) was added to the medium to eliminate METs.

Reactive oxygen species (ROS) detection

Macrophages were inoculated for 24 h and treated with different concentrations of PS-NPs and BaP. After treatment, the cells were washed 3 times with PBS, and incubated with DCFH-DA (Solarbio) for 30 min, and the ROS levels were observed under a fluorescence microscope after PBS washing.

Co-culture of RAW264.7 and MLE-12 cells

To establish an in vitro alveolar barrier model, we used a co-culture system of MLE-12 and RAW264.7 cells. The cells were seeded in a 4:1 ratio in six-well plates: first, 3.0×10^5 MLE-12 cells were pre-plated per well and cultured for 4 hours, then 7.5×10^4 RAW264.7 cells were added (total of 3.75×10^5 cells per well). After co-culturing for 24 hours and ensuring adequate cell adhesion, drug interventions were carried out. After three washes with PBS, the cells were fixed in 4% paraformaldehyde. Immunofluorescence was used to detect inflammation and fibrosis markers.

Hydroxyproline assay

The HYP content in lung tissue homogenates was determined using a hydroxyproline assay kit. The procedure strictly followed the kit instructions (Nanjing Jiancheng Bioengineering Institute), with absorbance values measured at 550 nm using a microplate reader. HYP quantitative analysis: to enhance the reliability of this new test, the sample size is set at n=6 per group.

Endoplasmic reticulum calcium ion fluorescence staining

After 24 h of treatment with PS-NPs and BaP, the cells were washed three times with PBS

and stained with Hank's Balanced Salt Solution (HBSS/Ca/Mg) containing Ca^{2+}, Mg^{2+}, diluted with 1 μM ER-Tracker Red (BODIPY® TR Glibenclamide) and Fluo-4 AM (Aladdin) working solution. The cells were incubated for 30 min at 37 °C, washed with PBS, and observed under a fluorescence microscope.

Use of inhibitors

Nifedipine (0.2 μM; Yeasen) was used as a calcium channel inhibitor.

Fluorescent immunostaining

Cells treated with PS-NPs and BaP for 24 h were washed twice with PBS and fixed with 4% paraformaldehyde for 30 min. After washing with PBS, the cells were treated with 0.5% Triton X-100 for 8 min at room temperature, washed twice with PBS, and incubated with goat serum sealant at 37 °C for 40 min. The cells were then stained with a primary antibody against il-1β (Nifedipine), which was used as a calcium channel inhibitor. Primary antibodies (Abways, China) il-1β, TNF-α, MMP9, H3, MPO, α-SMA, E-cadherin, E-cadherin, Collagen 1, etc., were incubated at 4°C overnight then washed with PBS, added with direct standard secondary antibody, and incubated at 37°C for 1 h. After washing with PBS, the nuclei were stained by Hoechst for 10 min avoiding light, blocked with 10% glycerol, and visualized by fluorescence microscope.

Quantitative real-time PCR (real-time quantitative PCR)

RNA was extracted by adding 1 mL of TRIzol to 50 mg of lung tissue, reverse transcribed to cDNA using a commercial kit (AG11728, ACCURATE BIOTECHNOLOGY (HUNAN) CO., LTD, Changsha, China), and stored at -80°C. Primer sequences were designed online (Sangon

Biotech) and mRNA expression levels were detected. β-actin was used as an internal reference gene, and the data were normalized to $2^{-\Delta\Delta Ct}$.

Western blotting

Lung tissues and cultured cells were lysed in pre-cooled RIPA lysate containing protease inhibitor (100:1), ground, and centrifuged for supernatant. Proteins were denatured, separated using SDS-PAGE gels, and transferred to PVDF membranes. After blocking with BSA for 2 hours, membranes were washed 3 times with TBST, and incubated with primary antibodies overnight at 4°C. incubated with secondary antibodies for 1 h. After incubation, they were washed three times with TBST, developed for 1 min with ultrasensitive developer , photographed with a gel imaging system, and quantified using Image J quantitative grey scale values. Primary antibodies used in this study are listed in Supplementary Table 2, and the replicated Western blot results are provided in Supplementary Figure 6

Statistical analysis

Data analysis was performed using GraphPad Prism 9. Comparisons between groups were based on the sample sizes set in each experiment, with data obtained from at least three independent experiments and expressed as mean ± standard deviation. Differences between groups were assessed using one-way ANOVA, and $p < 0.05$ was considered statistically significant. Abbreviations used in this study are defined in table 2.

Acknowledgments

This work was supported by the Major Science and Technology plan of Hainan Province (ZDYF2022SHFZ321), National Natural Science Foundation of China (42377273), Research start-up Project of Hainan University (XJ2300009832), Hainan Provincial Graduate Innovation Research Project (SA2400003272).Hainan Province Science and Technology Special Fund (ZDYF2022SHFZ321). We would like to express our gratitude to the Biorender website (https://app.biorender.com/) for providing resources for creating illustrations.

Competing interests

The authors declare no competing interests.

Author contributions

Yu Chen: Conceptualization, Writing-Original Draft, Formal analysis, Data Curation, Methodology, Data Curation,

Yingai Zhang: Project administration, Resources

Yuting Zhang: Methodology

Xu Zhang: Data Curation

Shuguo Lv: Revision, Resource

Mohamed Mohsen: Methodology, Writing - Review & Editing

Kai Yin : Supervision, Methodology

Xiaoshan Zhu：Resource

Hailong Zhou: Supervision, Funding acquisition

Data availability

All data supporting the findings are included in the paper and its supplementary files. All raw data are provided in the supplementary information. Sequencing reads are deposited in NCBI SRA under accession PRJNA1401317. Additional data are available from the corresponding author upon reasonable request.

References

[1] ROLAND G, JENNA R J, KARA LAVENDER L. Production, use, and fate of all plastics ever made [J]. Science Advances, 2017, 3(7): e1700782.

[2] GIGAULT J, HALLE A T, BAUDRIMONT M, et al. Current opinion: What is a nanoplastic? [J]. Environmental Pollution, 2018, 235: 1030-4.

[3] RICHARD C T, YLVA O, RICHARD P M, et al. Lost at Sea: Where Is All the Plastic? [J]. Science (New York, NY), 2004, 304(5672): 838-.

[4] SAHA S C, SAHA G. Effect of microplastics deposition on human lung airways: A review with computational benefits and challenges [J]. Heliyon, 2024, 10(2).

[5] MERGA L B, REDONDO-HASSELERHARM P E, VAN DEN BRINK P J, et al. Distribution of microplastic and small macroplastic particles across four fish species and sediment in an African lake [J]. Science of The Total Environment, 2020, 741.

[6] GONZáLEZ-SOTO N, HATFIELD J, KATSUMITI A, et al. Impacts of dietary exposure to different sized polystyrene microplastics alone and with sorbed benzo[a]pyrene on biomarkers and whole organism responses in mussels Mytilus galloprovincialis [J]. Science of The Total Environment, 2019, 684: 548-66.

[7] GAO W, ZHANG P, WANG H, et al. From water to sediment: A meta-analysis of microplastic distribution and the impact of dams in reservoir ecosystems [J]. Eco-Environment & Health, 2025, 4(4).

[8] FENG M, LUO J, WAN Y, et al. Polystyrene Nanoplastic Exposure Induces Developmental Toxicity by Activating the Oxidative Stress Response and Base Excision Repair Pathway in Zebrafish (Danio rerio) [J]. ACS Omega, 2022, 7（36）: 32153-63.

[9] WARING R H, HARRIS R M, MITCHELL S C. Plastic contamination of the food chain: A threat to human health? [J]. Maturitas, 2018, 115: 64-8.

[10] ENYOH C E, VERLA A W, VERLA E N, et al. Airborne microplastics: a review study on method for analysis, occurrence, movement and risks [J]. Environmental Monitoring and Assessment, 2019, 191(11): 668.

[11] JOANA CORREIA P, JOãO P, ISABEL L, et al. Environmental exposure to microplastics: An overview on possible human health effects [J]. Science of The Total Environment, 2020, 702: 134455.

[12] ZEKANG L, SHUXIANG Z, QIAN L, et al. Polystyrene microplastics cause cardiac fibrosis by activating Wnt/β-catenin signaling pathway and promoting cardiomyocyte apoptosis in rats [J]. Environmental Pollution, 2020, 265: 115025.

[13] XIAOQI Z, CHUANXUAN W, XIAOYU D, et al. Micro- and nanoplastics: A new cardiovascular risk factor? [J]. Environment International, 2023, 171: 107662.

[14] FENG Y, TU C, LI R, et al. A systematic review of the impacts of exposure to micro- and nano-plastics on human tissue accumulation and health [J]. Eco-Environment & Health, 2023, 2(4): 195-207.

[15] JI Y, WANG Y, SHEN D, et al. Mucin corona delays intracellular trafficking and alleviates cytotoxicity of nanoplastic-benzopyrene combined contaminant [J]. Journal of Hazardous Materials, 2021, 406: 124306.

[16] DA SILVA BRITO W A, RAVANDEH M, SAADATI F, et al. Sonicated polyethylene terephthalate nano- and micro-plastic-induced inflammation, oxidative stress, and autophagy in vitro [J]. Chemosphere, 2024, 355: 141813.

[17] KUMAR R, MANNA C, PADHA S, et al. Micro(nano)plastics pollution and human health: How plastics can induce carcinogenesis to humans? [J]. Chemosphere, 2022, 298: 134267.

[18] CAMACHO M, HERRERA A, GóMEZ M, et al. Organic pollutants in marine plastic debris from Canary Islands beaches [J]. Science of The Total Environment, 2019, 662: 22-31.

[19] WANG F, WONG C S, CHEN D, et al. Interaction of toxic chemicals with microplastics: A critical review [J]. Water Research, 2018, 139: 208-19.

[20] BARNES D K A, GALGANI F, THOMPSON R C, et al. Accumulation and fragmentation of plastic debris in global environments [J]. Philosophical Transactions of the Royal Society B, 2009, 364(1526): 1985-98.

[21] LIU J M Y, ZHU D,ET AL. . Polystyrene Nanoplastics-Enhanced Contaminant Transport: Role of Irreversible Adsorption in Glassy Polymeric Domain [J]. Environmental Science and Ecotechnology, 2018, 52(5): 2677-85.

[22] THOMPSON R C, COURTENE-JONES W, BOUCHER J, et al. Twenty years of microplastic pollution research—what have we learned? [J]. Science (New York, NY), 2024, 386(6720): eadl2746.

[23] PITTURA L, AVIO C G, GIULIANI M E, et al. Microplastics as Vehicles of Environmental PAHs to Marine Organisms: Combined Chemical and Physical Hazards to the Mediterranean Mussels, Mytilus galloprovincialis [J]. Frontiers in Marine Science, 2018, 5.

[24] SUN N, WANG J, SHI H, et al. Compound effect and mechanism of oxidative damage induced by nanoplastics and benzo [a] pyrene [J]. Journal of Hazardous Materials, 2023, 460: 132513.

[25] ZHANG S Y, SHAO D, LIU H, et al. Metabolomics analysis reveals that benzo[a]pyrene, a component of PM(2.5), promotes pulmonary injury by modifying lipid metabolism in a phospholipase A2-dependent manner in vivo and in vitro [J]. Redox biology, 2017, 13: 459-69.

[26] DRIS R, GASPERI J, MIRANDE C, et al. A first overview of textile fibers, including microplastics, in indoor and outdoor environments [J]. Environmental Pollution, 2017, 221: 453-8.

[27] ZHI L, LI Z, SU Z, et al. Immunotoxicity of microplastics: Carrying pathogens and destroying the immune system [J]. TrAC Trends in Analytical Chemistry, 2024, 177: 117817.

[28] WU Q, LIU C, LIU D, et al. Polystyrene nanoplastics-induced lung apoptosis and ferroptosis via ROS-dependent endoplasmic reticulum stress [J]. Science of The Total Environment, 2024, 912: 169260.

[29] JIN W, ZHANG W, TANG H, et al. Microplastics exposure causes the senescence of human lung epithelial cells and mouse lungs by inducing ROS signaling [J]. Environment International, 2024, 185: 108489.

[30] LIN Y, XU H, WANG K, et al. Transcriptomics integrated with metabolomics reveals the effect of benzo[a]pyrene exposure on acute lung injury [J]. Ecotoxicology Environmental Safety, 2024, 288: 117323.

[31] THANNICKAL V J, TOEWS G B, WHITE E S, et al. Mechanisms of pulmonary fibrosis [J]. Annual Review of Medicine 2004, 55: 395-417.

[32] SOUMYAKRISHNAN S, AYARIGA J A, SREEPRIYA M, et al. Role of Immune Cells in the Initiation and Progression of Pulmonary Fibrosis [J]. Critical reviews in immunology, 2022, 42(5): 21-41.

[33] ZHAO L, SHI W, HU F, et al. Prolonged oral ingestion of microplastics induced inflammation in the liver tissues of C57BL/6J mice through polarization of macrophages and increased infiltration of natural killer cells [J]. Ecotoxicology and Environmental Safety, 2021, 227: 112882.

[34] YANG Q, DAI H, CHENG Y, et al. Oral feeding of nanoplastics affects brain function of mice by inducing macrophage IL-1 signal in the intestine [J]. Cell reports, 2023, 42(4): 112346.

[35] TARASCO M, GAVAIA P J, BENSIMON-BRITO A, et al. New insights into benzo[α]pyrene osteotoxicity in zebrafish [J]. Ecotoxicology and Environmental Safety, 2021, 226: 112838.

[36] JANG H J, MIN H Y, KANG Y P, et al. Tobacco-induced hyperglycemia promotes lung cancer progression via cancer cell-macrophage interaction through paracrine IGF2/IR/NPM1-driven PD-L1 expression [J]. Nature communications, 2024, 15(1): 4909.

[37] SADEGHI M, DEHNAVI S, JAMIALAHMADI T, et al. Neutrophil extracellular trap: A key player in the pathogenesis of autoimmune diseases [J]. International immunopharmacology, 2023, 116: 109843.

[38] YIN K, WANG D, ZHANG Y, et al. Polystyrene microplastics promote liver inflammation by inducing the formation of macrophages extracellular traps [J]. Journal of Hazardous Materials, 2023, 452: 131236.

[39] WANG S, CHEN L, SHI X, et al. Polystyrene microplastics-induced macrophage extracellular traps contributes to liver fibrotic injury by activating ROS/TGF-β/Smad2/3 signaling axis [J]. Environmental Pollution, 2023, 324: 121388.

[40] ZHANG Y, MEN J, YIN K, et al. Activation of gut metabolite ACSL4/LPCAT3 by microplastics in drinking water mediates ferroptosis via gut-kidney axis [J]. Communications biology, 2025, 8(1): 211.

[41] YANG D, LIU D, QIN M, et al. Intestinal Mucin Induces More Endocytosis but Less Transcytosis of Nanoparticles across Enterocytes by Triggering Nanoclustering and Strengthening the Retrograde Pathway [J]. ACS Applied Materials & Interfaces, 2018, 10(14): 11443-56.

[42] REN H, YIN K, LU X, et al. Synergy between nanoplastics and benzo[a]pyrene promotes senescence by aggravating ferroptosis and impairing mitochondria integrity in Caenorhabditis elegans [J]. Science of The Total Environment, 2024, 946: 174418.

[43] SAMUEL C S, BENNETT R G. Relaxin as an anti-fibrotic treatment: Perspectives, challenges and future directions [J]. Biochemical pharmacology, 2022, 197: 114884.

[44] YANG M, LIU Q, XUAN A. Relaxin-2 Alleviates Hyperoxia-Induced Acute Lung Injury in Neonatal Rats by Inhibiting TLR4/NF-κB [J]. Chemical biology & drug design, 2025, 105(6): e70140.

[45] HUANG X, GAI Y, YANG N, et al. Relaxin regulates myofibroblast contractility and protects against lung fibrosis [J]. American Journal Of Pathology, 2011, 179(6): 2751-65.

[46] HALLS M L. Constitutive formation of an RXFP1-signalosome: a novel paradigm in GPCR function and regulation [J]. Br J Pharmacol, 2012, 165(6): 1644-58.

[47] KERN A, BRYANT-GREENWOOD G D. Characterization of relaxin receptor (RXFP1) desensitization and internalization in primary human decidual cells and RXFP1-transfected HEK293 cells [J]. Endocrinology, 2009, 150(5): 2419-28.

[48] LIN D, LUO H, DONG B, et al. FOXO3a Induces Myocardial Fibrosis by Upregulating Mitophagy [J]. Frontiers in bioscience (Landmark edition), 2024, 29(2): 56.

[49] BENNETT R G. Relaxin and its role in the development and treatment of fibrosis [J]. Translational Research, 2009, 154(1): 1-6.

[50] YUAN Y, ZHANG Y, HAN X, et al. Relaxin alleviates TGFβ1-induced cardiac fibrosis via inhibition of Stat3-dependent autophagy [J]. Biochemical and biophysical research communications, 2017, 493(4): 1601-7.

[51] FANG C, ZENG Z, NI B, et al. Fibroblast PI3K/AKT signaling and extracellular matrix homeostasis: mechanisms, targets, and delivery challenges [J]. Frontiers in cell and developmental biology, 2025, 13: 1681875.

[52] AHMAD N, WANG W, NAIR R, et al. Relaxin induces matrix-metalloproteinases-9 and -13 via RXFP1: induction of MMP-9 involves the PI3K, ERK, Akt and PKC-ζ pathways [J]. Molecular and cellular endocrinology, 2012, 363(1-2): 46-61.

[53] LAM M, ROYCE S G, SAMUEL C S, et al. Serelaxin as a novel therapeutic opposing fibrosis and contraction in lung diseases [J]. Pharmacology & therapeutics, 2018, 187: 61-70.

[54] SINGH S, SIMPSON R L, BENNETT R G. Relaxin activates peroxisome proliferator-activated receptor γ (PPARγ) through a pathway involving PPARγ coactivator 1α (PGC1α) [J]. Journal Of Biological Chemistry, 2015, 290(2): 950-9.

[55] QI F, LV Z D, HUANG W D, et al. LncRNA TUG1 promotes pulmonary fibrosis progression via up-regulating CDC27 and activating PI3K/Akt/mTOR pathway [J]. Epigenetics, 2023, 18(1): 2195305.

[56] HU X, XU Q, WAN H, et al. PI3K-Akt-mTOR/PFKFB3 pathway mediated lung fibroblast aerobic glycolysis and collagen synthesis in lipopolysaccharide-induced pulmonary fibrosis [J]. Laboratory Investigation, 2020, 100(6): 801-11.

[57] CHEN L. Inflammatory responses and inflammation-associated diseases
in organs [J]. Oncotarget, 2018.

[58] ZHANG X, WANG S, LING L, et al. The distribution and structural fingerprints of metals from particulate matters (PM) deposited in human lungs [J]. Ecotoxicology and Environmental Safety, 2022, 233.

[59] LIU S, LIU L, WANG Y, et al. Assessing inhalation exposure to infectious particles in hospitals using a breathing thermal manikin [J]. Chinese Science Bulletin, 2023, 69: 1234~44.

[60] WANG Z, YANG X, MEI X, et al. SARS-CoV-2-specific CD4+ T cells are associated with long-term persistence of neutralizing antibodies [J]. Signal transduction and targeted therapy, 2022, 7(1).

[61] BRINKMANN V, REICHARD U, GOOSMANN C, et al. Neutrophil extracellular traps kill bacteria [J]. Science (New York, NY), 2004, 303(5663): 1532-5.

[62] ARIAS A H, ALVAREZ G, POZO K, et al. Beached microplastics at the Bahia Blanca Estuary (Argentina): Plastic pellets as potential vectors of environmental pollution by POPs [J]. Marine Pollution Bulletin, 2023, 187: 114520.

[63] SCHMIDT A, MüHL M, BRITO W A, et al. Antioxidant Defense in Primary Murine Lung Cells following Short- and Long-Term Exposure to Plastic Particles [J]. Antioxidants, 2023, 12(2).

[64] ARORA S, DEV K, AGARWAL B, et al. Macrophages: Their role, activation and polarization in pulmonary diseases [J]. Immunobiology, 2018, 223(4): 383-96.

[65] WANG X, REN X M, HE H, et al. Cytotoxicity and pro-inflammatory effect of polystyrene nano-plastic and micro-plastic on RAW264.7 cells [J]. Toxicology, 2023, 484: 153391.

[66] RASMUSSEN K H, HAWKINS C A-O. Role of macrophage extracellular traps in innate immunity and inflammatory disease [J]. Biochemical Society Transactions, 2022, 50(1)(1470-8752 (Electronic)): 21-32.

[67] ZHANG J, DU J, LIU D, et al. Polystyrene microplastics induce pulmonary fibrosis by promoting alveolar epithelial cell ferroptosis through cGAS/STING signaling [J]. Ecotoxicol Environ Saf, 2024, 277: 116357.

[68] BRINKMANN V, ZYCHLINSKY A. Entering the neutrophil trap [J]. Nature reviews Immunology, 2021, 21(10): 615.

[69] KUMMARAPURUGU A B, ZHENG S, MA J, et al. Neutrophil Elastase Triggers the Release of Macrophage Extracellular Traps: Relevance to Cystic Fibrosis [J]. American Journal of Respiratory Cell and Molecular Biology, 2022, 66(1): 76-85.

[70] VAARMANN A, GANDHI S, ABRAMOV A Y. Dopamine induces Ca2+ signaling in astrocytes through reactive oxygen species generated by monoamine oxidase [J]. Journal Of Biological Chemistry, 2010, 285(32): 25018-23.

[71] WU S, YANG J, SUN G, et al. Macrophage extracellular traps aggravate iron overload-related liver ischaemia/reperfusion injury [J]. British Journal of Pharmacology, 2021, 178(18): 3783-96.

[72] YANG J, LI Y, BHALLA A, et al. A novel co-culture model for investigation of the effects of LPS-induced macrophage-derived cytokines on brain endothelial cells [J]. PloS one, 2023, 18(7): e0288497.

[73] DONG C D, CHEN C W, CHEN Y C, et al. Polystyrene microplastic particles: In vitro pulmonary toxicity assessment [J]. Journal of Hazardous Materials, 2020, 385: 121575.

[74] WOO J H, SEO H J, LEE J Y, et al. Polypropylene nanoplastic exposure leads to lung inflammation through p38-mediated NF-κB pathway due to mitochondrial damage [J]. Part Fibre Toxicol, 2023, 20(1): 2.

[75] FAN J, LIU L, LU Y, et al. Acute exposure to polystyrene nanoparticles promotes liver injury by inducing mitochondrial ROS-dependent necroptosis and augmenting macrophage-hepatocyte crosstalk [J]. Part Fibre Toxicol, 2024, 21(1): 20.

[76] HU M, PALIĆ D. Micro- and nano-plastics activation of oxidative and inflammatory adverse outcome pathways [J]. Redox biology, 2020, 37: 101620.

[77] GODA C, BALLI D, BLACK M, et al. Loss of FOXM1 in macrophages promotes pulmonary fibrosis by activating p38 MAPK signaling pathway [J]. PLoS genetics, 2020, 16(4): e1008692.

[78] FORTIER S M, WALKER N M, PENKE L R, et al. MAPK phosphatase 1 inhibition of p38α within lung myofibroblasts is essential for spontaneous fibrosis resolution [J]. Journal Of Clinical Investigation, 2024, 134(10): e172826.

[79] CHEN J, CHEN X, XUAN Y, et al. Surface functionalization-dependent inflammatory potential of polystyrene nanoplastics through the activation of MAPK/ NF-κB signaling pathways in macrophage Raw 264.7 [J]. Ecotoxicology and Environmental Safety, 2023, 251: 114520.

[80] HUANG G, YANG X, YU Q, et al. Overexpression of STX11 alleviates pulmonary fibrosis by inhibiting fibroblast activation via the PI3K/AKT/mTOR pathway [J]. Signal transduction and targeted therapy, 2024, 9(1): 306.

[81] SHEN S, SUN T, DING X, et al. The exoprotein Gbp of Fusobacterium nucleatum promotes THP-1 cell lipid deposition by binding to CypA and activating PI3K-AKT/MAPK/NF-κB pathways [J]. Journal of advanced research, 2024, 57: 93-105.

[82] KANAI A J, KONIECZKO E M, BENNETT R G, et al. Relaxin and fibrosis: Emerging targets, challenges, and future directions [J]. Molecular and cellular endocrinology, 2019, 487: 66-74.

[83] WU J, LIU Q, ZHANG X, et al. The interaction between STING and NCOA4 exacerbates lethal sepsis by orchestrating ferroptosis and inflammatory responses in macrophages [J]. Cell Death & Disease, 2022, 13(7).

[84] DMELLO C, ZHAO J, CHEN L, et al. Checkpoint kinase 1/2 inhibition potentiates anti-tumoral immune response and sensitizes gliomas to immune checkpoint blockade [J]. Nature communications, 2023, 14(1).

[85] HEGEDŰS C, JUHáSZ T, FIDRUS E, et al. Cyclobutane pyrimidine dimers from UVB exposure induce a hypermetabolic state in keratinocytes via mitochondrial oxidative stress [J]. Redox biology, 2021, 38.

[86] LOU X, WANG J, JIN X, et al. An oral bacterial pyroptosis amplifier against malignant colon cancer [J]. Nano Today, 2024, 54.

[87] WINSLOW S, ODQVIST L, DIVER S, et al. Multi-omics links IL-6 trans-signalling with neutrophil extracellular trap formation andHaemophilusinfection in COPD [J]. European Respiratory Journal, 2021, 58(4).

Figure Legend

Figure 1. PS-MPs and BaP co-exposure induce lung inflammation and fibrosis damage. A: Body weight changes in mice over 16 weeks. B: Changes in lung organ coefficients over 16 weeks. Con: Control group; PS-NPs: Polystyrene nanoparticle treatment group; BaP: Benzo[a]pyrene treatment group; Mix: Co-exposure group (n=5). C: H&E staining of lung tissue. Scale bar: 50 μm. D: Results of antioxidant function detection in lung tissues of control and treatment groups. E and F: Levels of inflammation-related proteins in lung tissues (IL-1β, TNF-α). G: Masson's trichrome staining to detect lung tissue fibrosis (a. Con b. BaP c. PS-NPs d. Mix), 200X. H: Levels of fibrosis-related proteins in lung tissues (Collagen I, α-SMA, S100A9). (n=3) . I.Expression levels of HYP (n=6). Results are expressed as mean ± SD. * $P < 0.05$, ** $P < 0.01$, *** $P < 0.001$.

Figure 2. PS-MPs and BaP induce the production of METs. A and B: Cell viability after exposure to different concentrations of PS-NPs and BaP measured by CCK8 assay (n=5). C: Lipopolysaccharide as a positive inducer, nuclei stained with Hochest, detecting the formation of METs. D: ROS levels detected using DCFH-DA fluorescent probe. E: Relative protein expression levels of Cith3 in RAW264.7 cells treated with BaP or PS-MPs alone and in combination, using immunofluorescence detection (N = 3), with lipopolysaccharide as a positive inducer. Results are expressed as mean ± SD. Scale bars: 100 or 50 μm. * $P < 0.05$, ** $P < 0.01$, *** $P < 0.001$.

Figure 3. Inflammation and fibrosis in lung cells induced by METs from co-exposure to PS-MPs

and BaP. A: Co-culture system of macrophages (Raw264.7) and lung epithelial cells (MLE-12). B: Detection of ROS levels in MLE-12 and RAW263.7 cells after exposure to PS-MPs, BaP, and Mix groups using DCFH-DA fluorescent probe for reactive oxygen species, with Rosup as the positive reagent. C: Immunofluorescence of Cith3 in the co-culture system of RAW264.7 cells and CLE-12 cells after different treatments, with Dnase I as the nuclear structure inhibitor. D: Relative protein expression levels of Collagen I in the immunofluorescence detection of co-culture systems of RAW264.7 and CLE-12 cells treated with BaP or PS-MPs alone and in combination. Results are presented as mean ± SD. * $P < 0.05$, ** $P < 0.01$, *** $P < 0.001$.

Figure 4 PS-MPs and BaP co-exposure activates the Relaxin signaling pathway A: Functional enrichment analysis of differentially expressed genes in the Mix group based on the GO database; B: Venn diagram analysis of the distribution of differentially expressed genes among groups; C: KEGG pathway enrichment analysis of the Con, BaP, and Mix groups. D-E: Protein levels related to the relaxin pathway (RXFP1, RXFP3, RXFP4). F: Relative mRNA expression levels of relaxin signaling pathway-related genes (RXFP1, RXFP3, RXFP4) (N = 3). Results are presented as mean ± SD. * $P < 0.05$, ** $P < 0.01$, *** $P < 0.001$.

Figure 5: The Relaxin 4 signaling pathway mediates METs formation via endoplasmic reticulum calcium ions. A: Fluorescence imaging of endoplasmic reticulum calcium ions in macrophages (red: endoplasmic reticulum; green: calcium ions; n=3; scale bar: 100 μm); B: Changes in protein

expression of key molecules PLC and IP3R in the endoplasmic reticulum calcium ion release pathway. C and D: Detection of marker proteins for METs in lung tissue (Cith3, MPO, MMP9). E: Endoplasmic reticulum calcium ion fluorescence images of the Mix group and Con group, with Nifedipine as a calcium ion chelator. (Scale bar: 100 μm). F: Changes in protein expression of key molecules PLC and IP3R in the endoplasmic reticulum calcium ion release pathway after the addition of a calcium ion chelator. Results are presented as mean ± SD. * $P < 0.05$, ** $P < 0.01$, *** $P < 0.001$.

Figure 6. Relaxin 1 and Relaxin 3 pathways regulate inflammation and fibrosis via PI3K-AKT, MAPK. A: Relative protein expression levels (PP38/P38, P-JNK/JNK, P-ERK/ERK) of Relaxin3 (MAPK signaling pathway) in lung tissues of Con and Mix exposed mice (N = 3). B and C: Relative protein expression levels (PPI3K/PI3K, P-AKT/AKT, P-κB/I-κB) of Relaxin1 (PI3K-AKT pathway/NF-κB signaling pathway) in lung tissues of Con and Mix exposed mice (N = 3). D: Relative mRNA expression levels of inflammation and PI3K-AKT, MAPK-related pathways (N=3). E: Relative protein expression levels (E-cadherin) of fibrosis in lung tissues of control and Mix exposed mice (N = 3). Results are presented as mean ± SD. * $P < 0.05$, ** $P < 0.01$, *** $P < 0.001$.

Table 1 Gene special primers used in the real-time quantitative reverse transcription PCR

Gene	Primer Sequence (5′ – 3′)
Relaxin1	Forward：AGGCAGAAACTTCCGAATGCT
	Reverse：ACAGCTCGTAAATTGGCTTCATC
Relaxin4	Forward：ATGCCAGCACCTTCCTAATCA
	Reverse：CCCCACAACTCAACTTCAGC
Relaxin3	Forward： GCGCAAATCCTCCATCAACC

	Reverse： TTCTCCACAGCCCAAAAGGG
il-1 β	Forward：TTCAGGCAGGCAGTATCACTC
	Reverse：GAAGGTCCACGGGAAAGACAC
TNF- α	Forward：CTGAACTTCGGGGTGATCGG
	Reverse：GGCTTGTCACTCGAATTTTGAGA
NF- κ B	Forward：AGAGGGGATTTCGATTCCGC
	Reverse：CCTGTGGGTAGGATTTCTTGTTC
PI3K	Forward：CGGAGAACCTATTGCGAGGG
	Reverse：TGCTTGACTTCGCCGTCTAC
AKT	Forward：CCTCAAGAACGATGGCACCT
	Reverse：TGCAGGCAGCGGATGATAAA
P38	Forward：TTGCTTTCTCTCCCGCACAAA
	Reverse：CATTATTGCCTTGCCCCAGC
JNK	Forward：TTGCTTTCTCTCCCGCACAAA
	Reverse：AGAGCCTGTTCAACTTCAATCC
ERK	Forward：ACAAGCGGTGCCATGAGTTCG
	Reverse：CGCAGTGGTCGCAGAAGGTG

Table 2 List of abbreviations and their full definitions

Abbreviation	Full term (definition)
MDA	malondialdehyde
T-AOC	total antioxidant capacity
GSH	reduced glutathione
GSSG	oxidized glutathione
SOD	superoxide dismutase
CAT	catalase
IL-1β	interleukin-1 beta
TNF-α	tumour necrosis factor-alpha
Collagen1	collagen type I
LPS	lipopolysaccharide
PMA	phorbol 12-myristate 13-acetate
CITH3	citrullinated histone H3
MPO	myeloperoxidase

Abbreviation	Full term (definition)
ROS	reactive oxygen species
S100A9	S100 calcium-binding protein A9
α-SMA	alpha-smooth muscle actin
MMP9	matrix metalloproteinase-9
METs	macrophage extracellular traps
RELAXIN	relaxin family peptide hormone
RXFP1-3	relaxin family peptide receptors 1–3
IP3-PLC	inositol 1,4,5-trisphosphate–phospholipase C pathway
MAPK	mitogen-activated protein kinase (JNK, ERK, p38)
PI3K-AKT	phosphatidylinositol-3-kinase–protein kinase B pathway
HYP	hydroxyproline
E-cadherin	epithelial cadherin

Editor's Summary

Co-exposure to polystyrene nanoplastics and benzo(a)pyrene exacerbates lung inflammation and fibrosis via Relaxin-Ca^{2+}–MET signalling, unveiling potential therapeutic targets.

Peer review statement

Communications Biology thanks Naresh Singh and the other, anonymous, reviewer(s) for their contribution to the peer review of this work. Primary Handling Editor: Dario Ummarino.

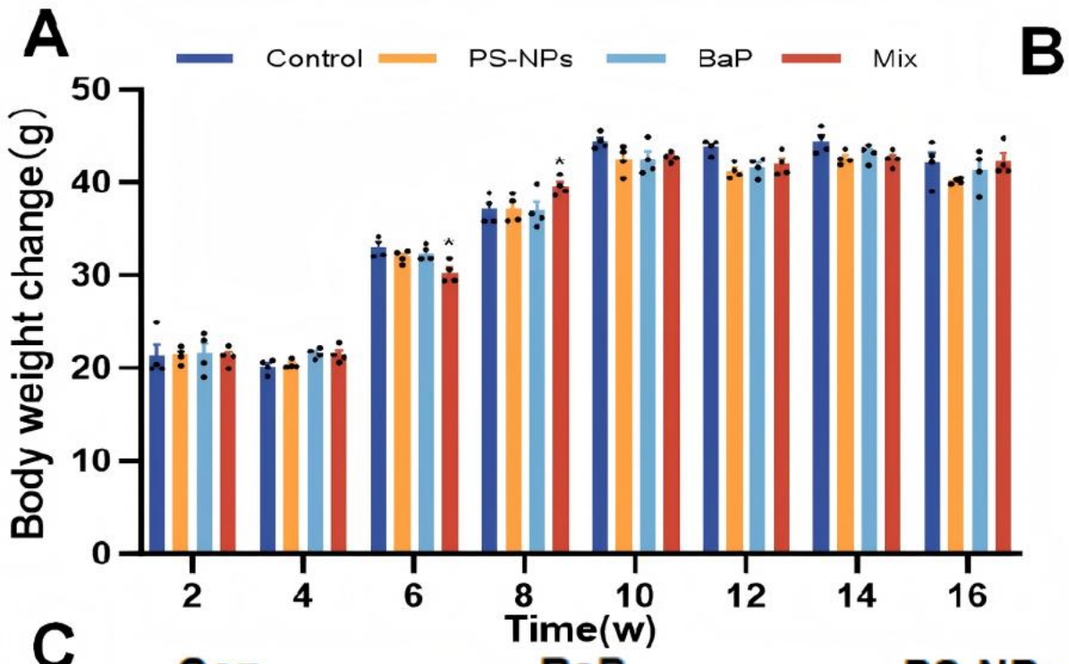
A
Control
PS-NPs
BaP
Mix
Body weight change(g)
Time(w)

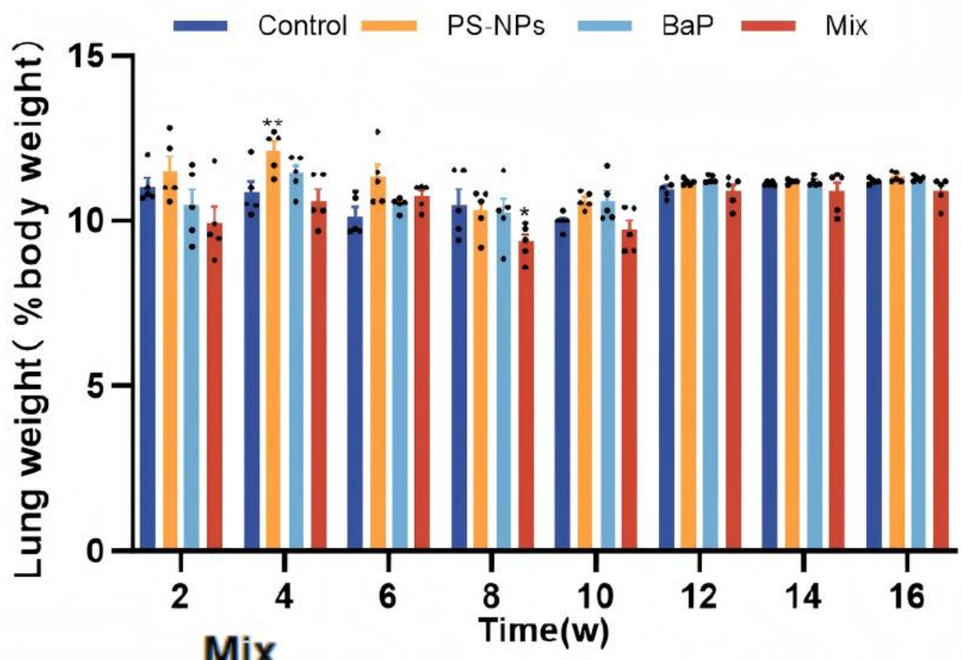
B
Control
PS-NPs
BaP
Mix
Lung weight(%body weight)
Time(w)

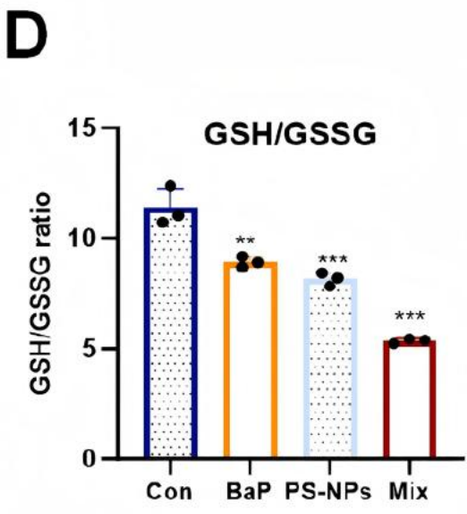
D
GSH/GSSG
GSH/GSSG ratio
Con
BaP
PS-NPs
Mix

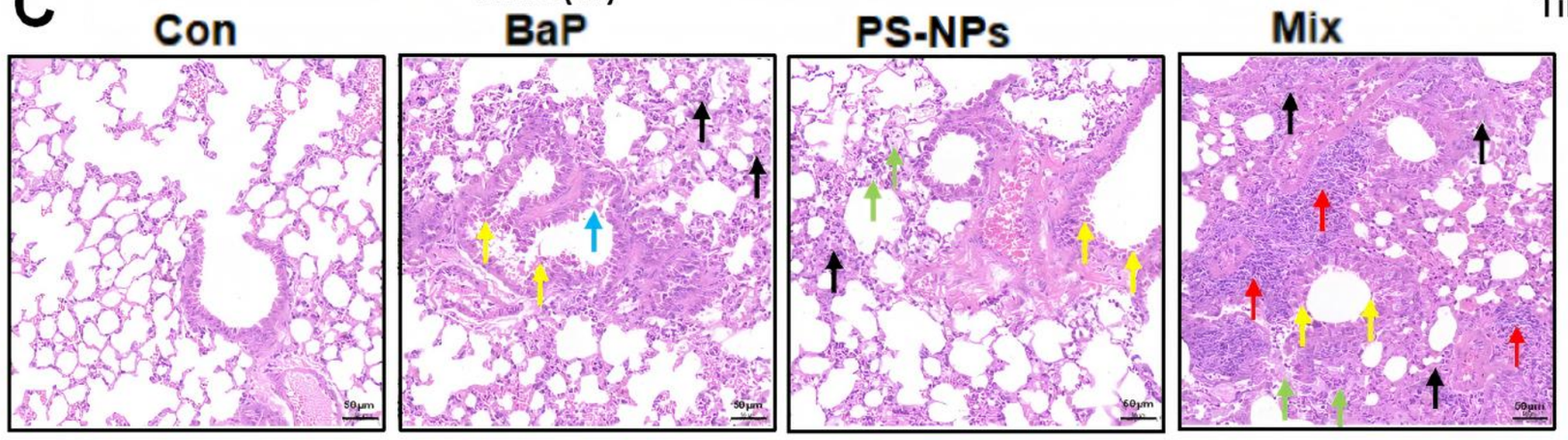
C
Con
BaP
PS-NPs
Mix

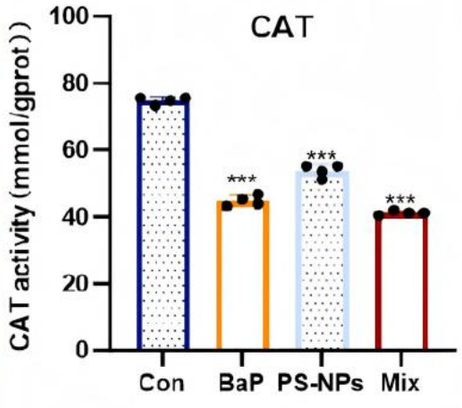
CAT
CAT activity (mmol/gprot))
Con
BaP
PS-NPs
Mix

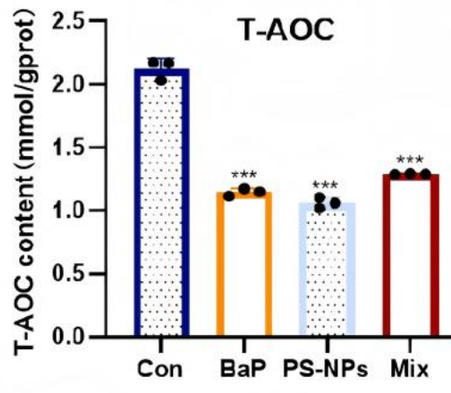
T-AOC
T-AOC content (mmol/gprot)
Con
BaP
PS-NPs
Mix

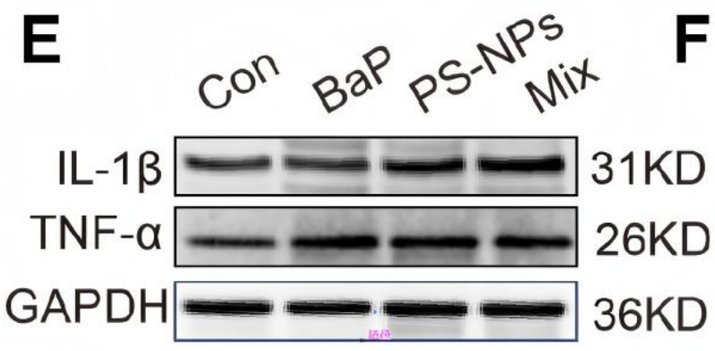
E
Con
BaP
PS-NPs
Mix
IL-1β
TNF-α
GAPDH
31KD
26KD
36KD

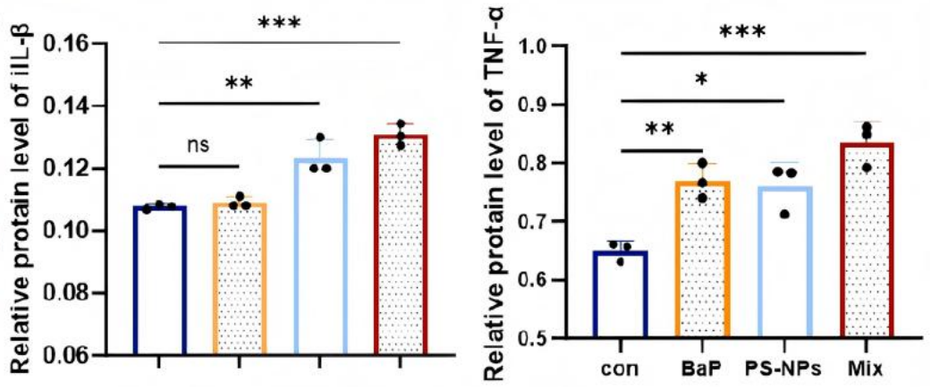
F
Relative protain level of IL-β
Relative protain level of TNF-α
con
BaP
PS-NPs
Mix

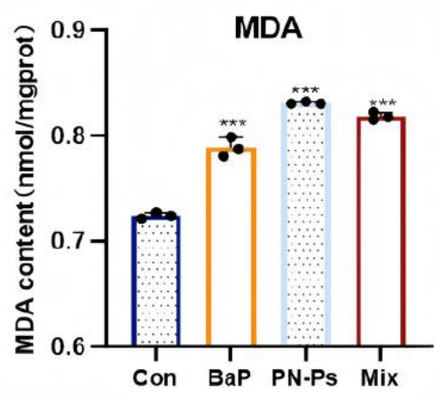
MDA
MDA content (nmol/mgprot)
Con
BaP
PN-Ps
Mix

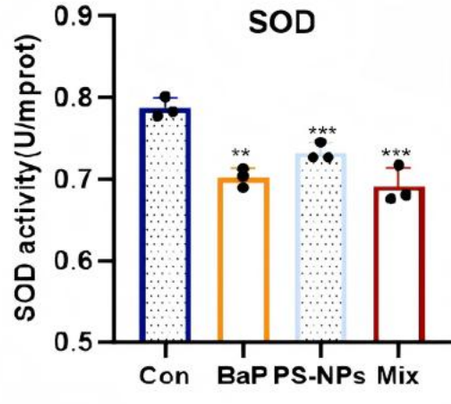
SOD
SOD activity(U/mprot)
Con
BaP
PS-NPs
Mix

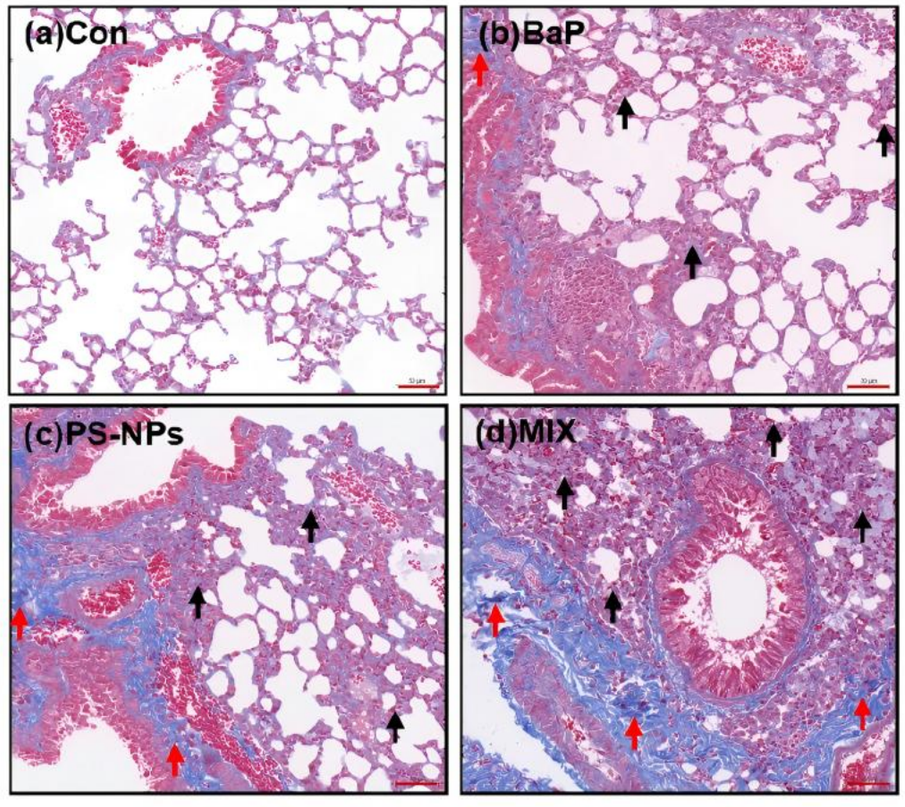
G
(a)Con
(b)BaP
(c)PS-NPs
(d)MIX

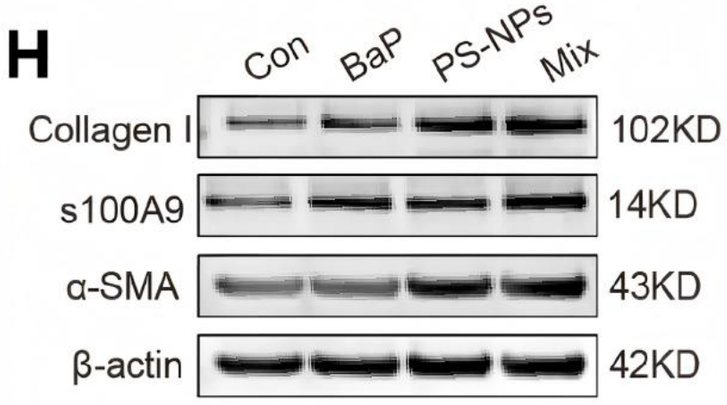
H
Con
BaP
PS-NPs
Mix
Collagen I
s100A9
α-SMA
β-actin
102KD
14KD
43KD
42KD

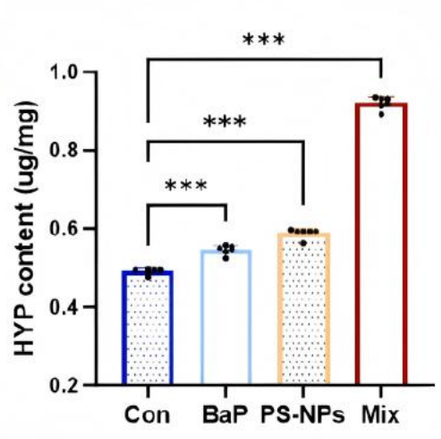
I
HYP content (ug/mg)
Con
BaP
PS-NPs
Mix

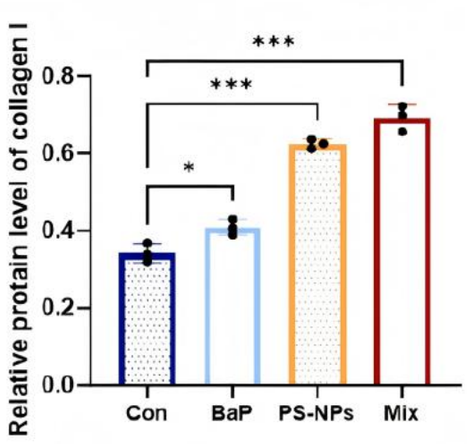
Relative protain level of collagen I
Con
BaP
PS-NPs
Mix

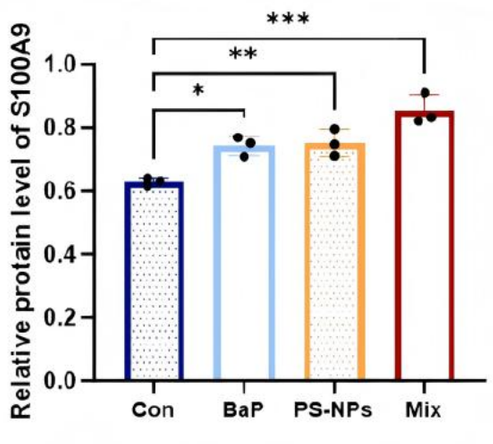
Relative protain level of S100A9
Con
BaP
PS-NPs
Mix

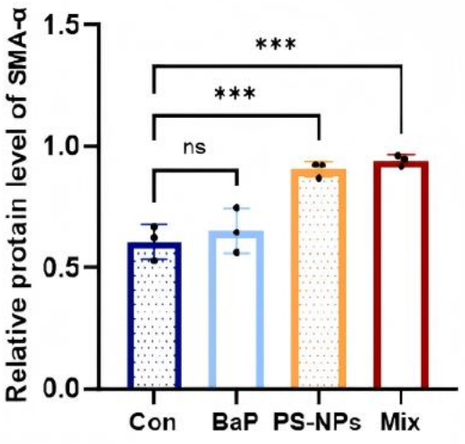
Relative protain level of SMA-α
Con
BaP
PS-NPs
Mix

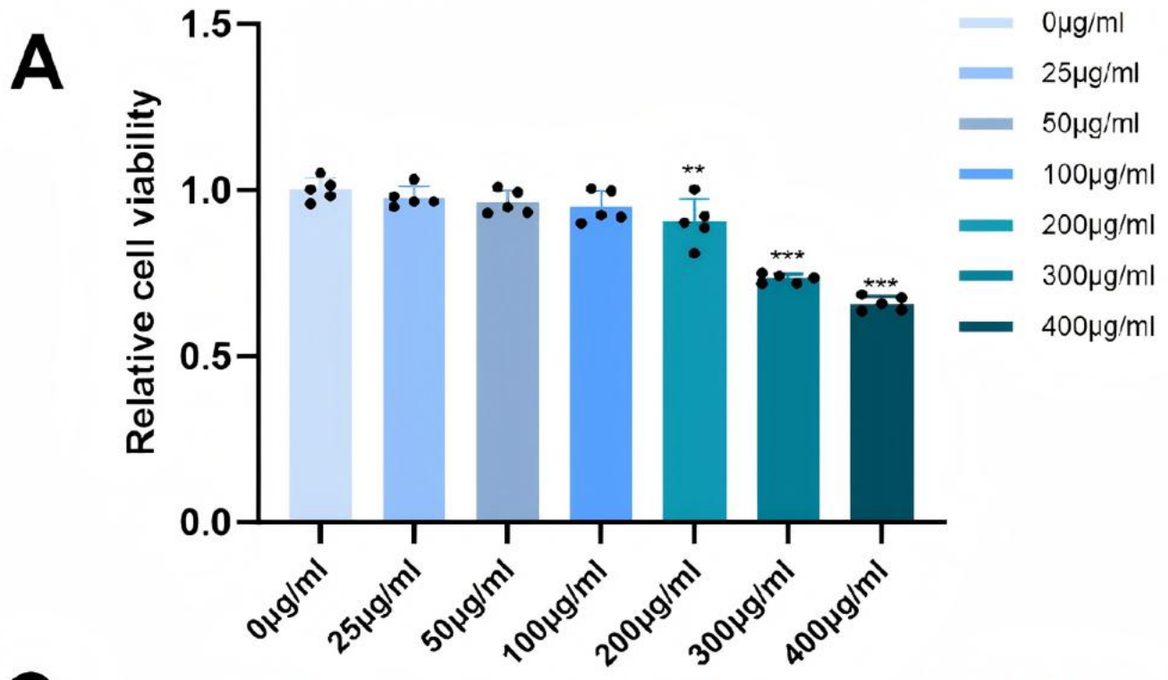
A
Relative cell viability
1.5
1.0
0.5
0.0
0μg/ml
25μg/ml
50μg/ml
100μg/ml
200μg/ml
300μg/ml
400μg/ml
**
***
***

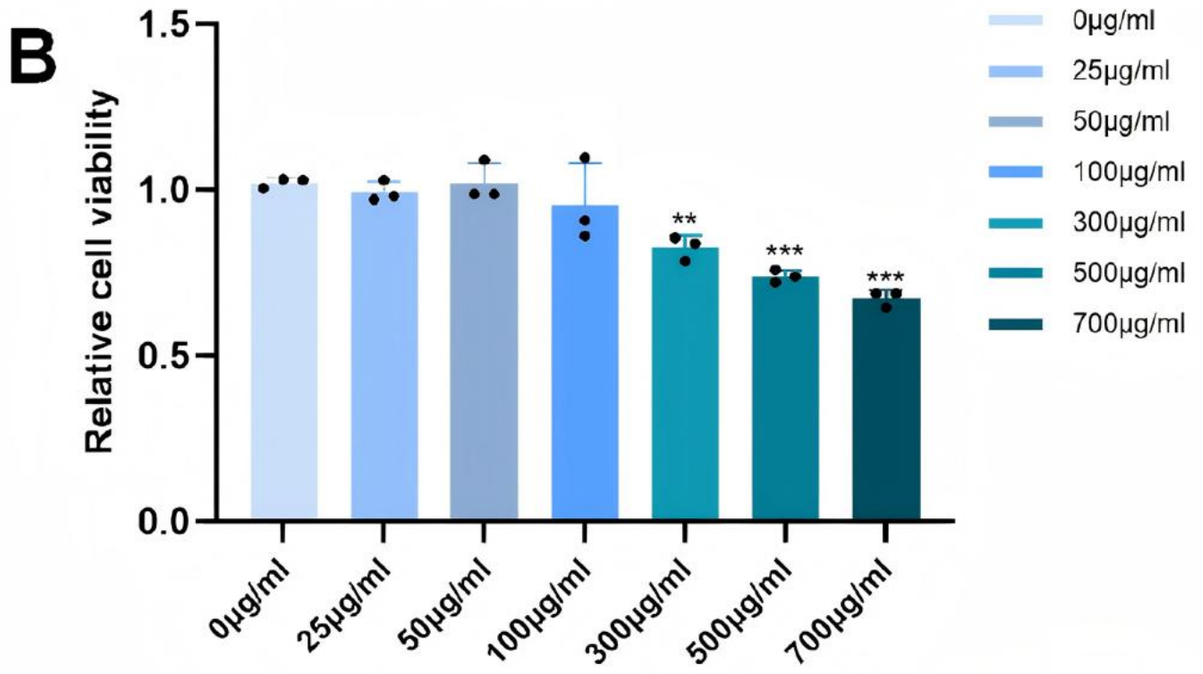
B
Relative cell viability
1.5
1.0
0.5
0.0
0μg/ml
25μg/ml
50μg/ml
100μg/ml
300μg/ml
500μg/ml
700μg/ml
**
***
***

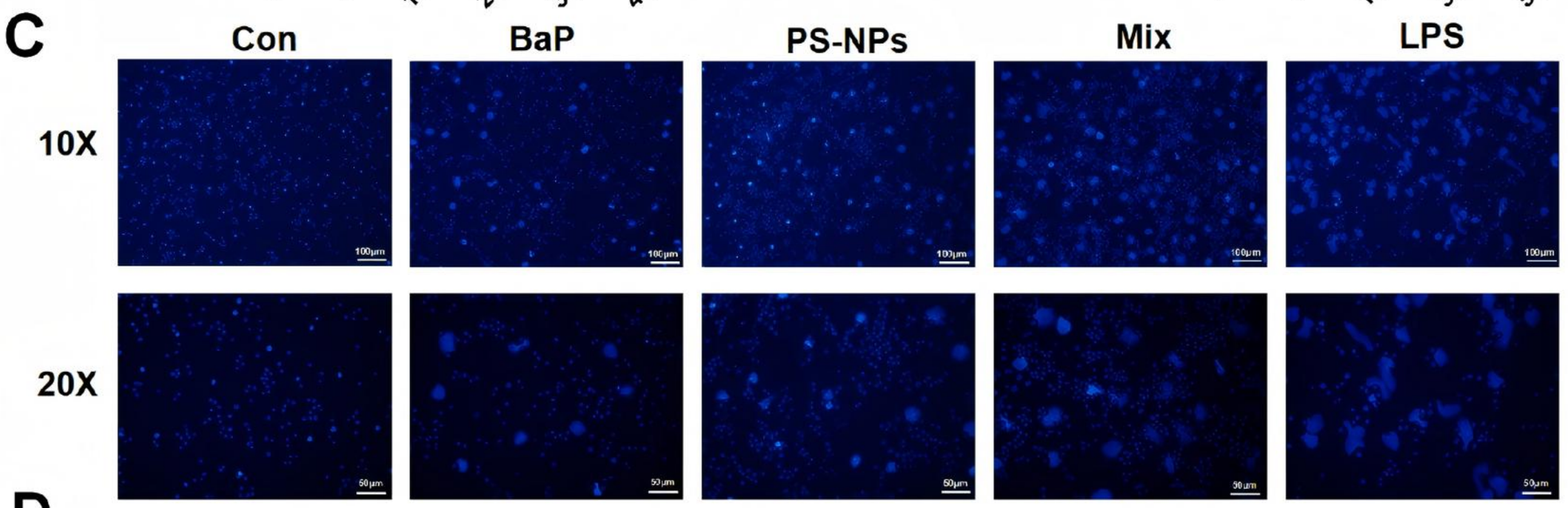
C
Con
BaP
PS-NPs
Mix
LPS
10X
20X
100μm
50μm

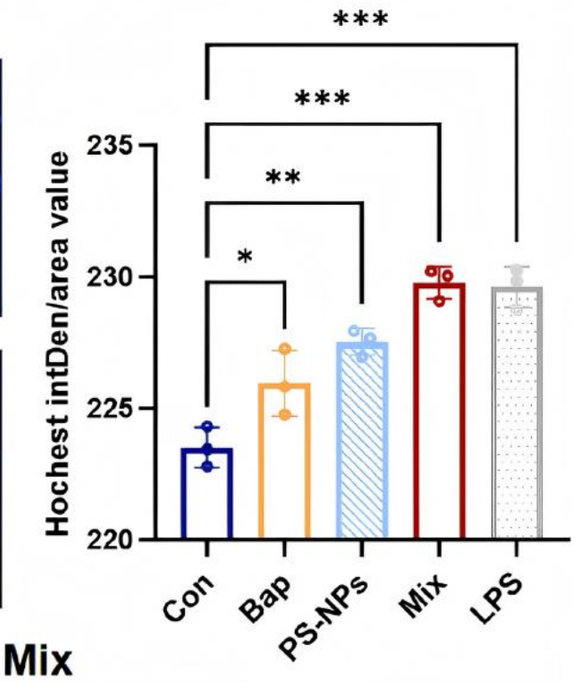
***
***
**
*
Hochest intDen/area value
235
230
225
220
Con
Bap
PS-NPs
Mix
LPS

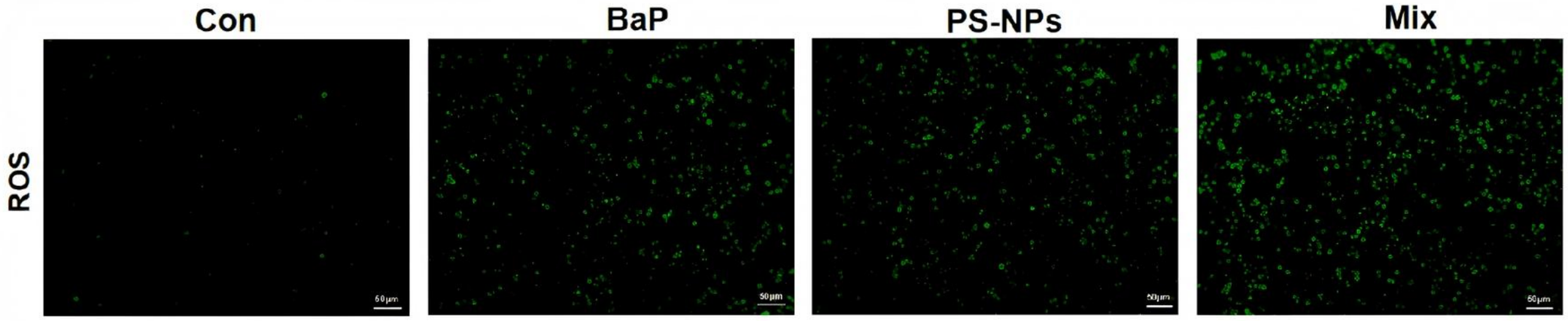
D
Con
BaP
PS-NPs
Mix
ROS
50μm

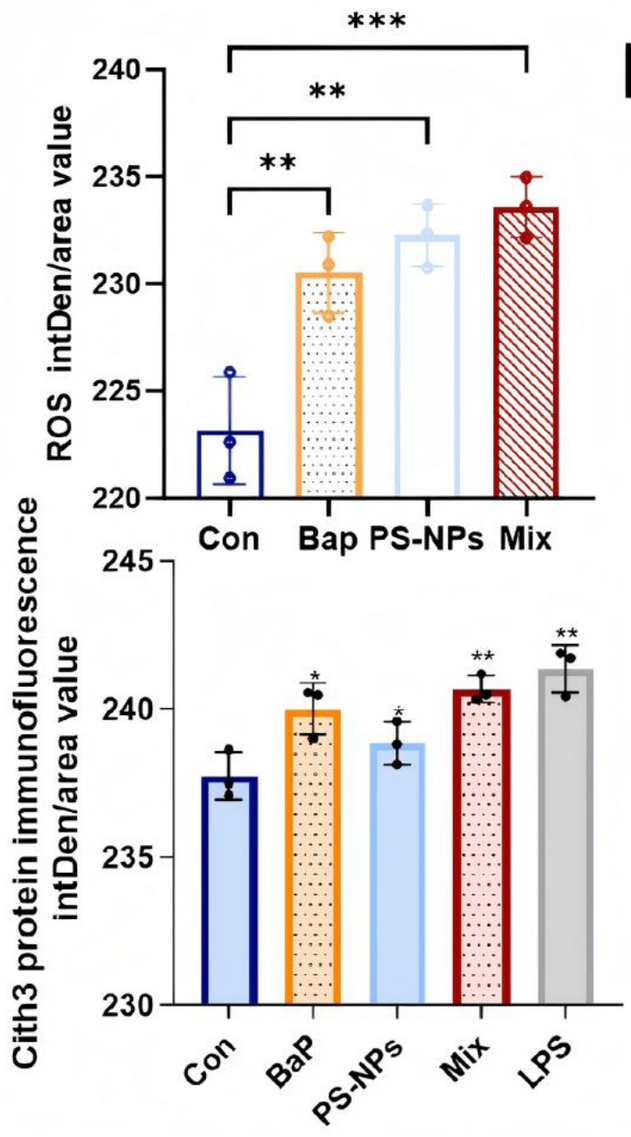
***
**
**
ROS intDen/area value
240
235
230
225
220
Con
Bap
PS-NPs
Mix
Cith3 protein immunofluorescence intDen/area value
245
240
235
230
*
*
**
**
Con
BaP
PS-NPs
Mix
LPS

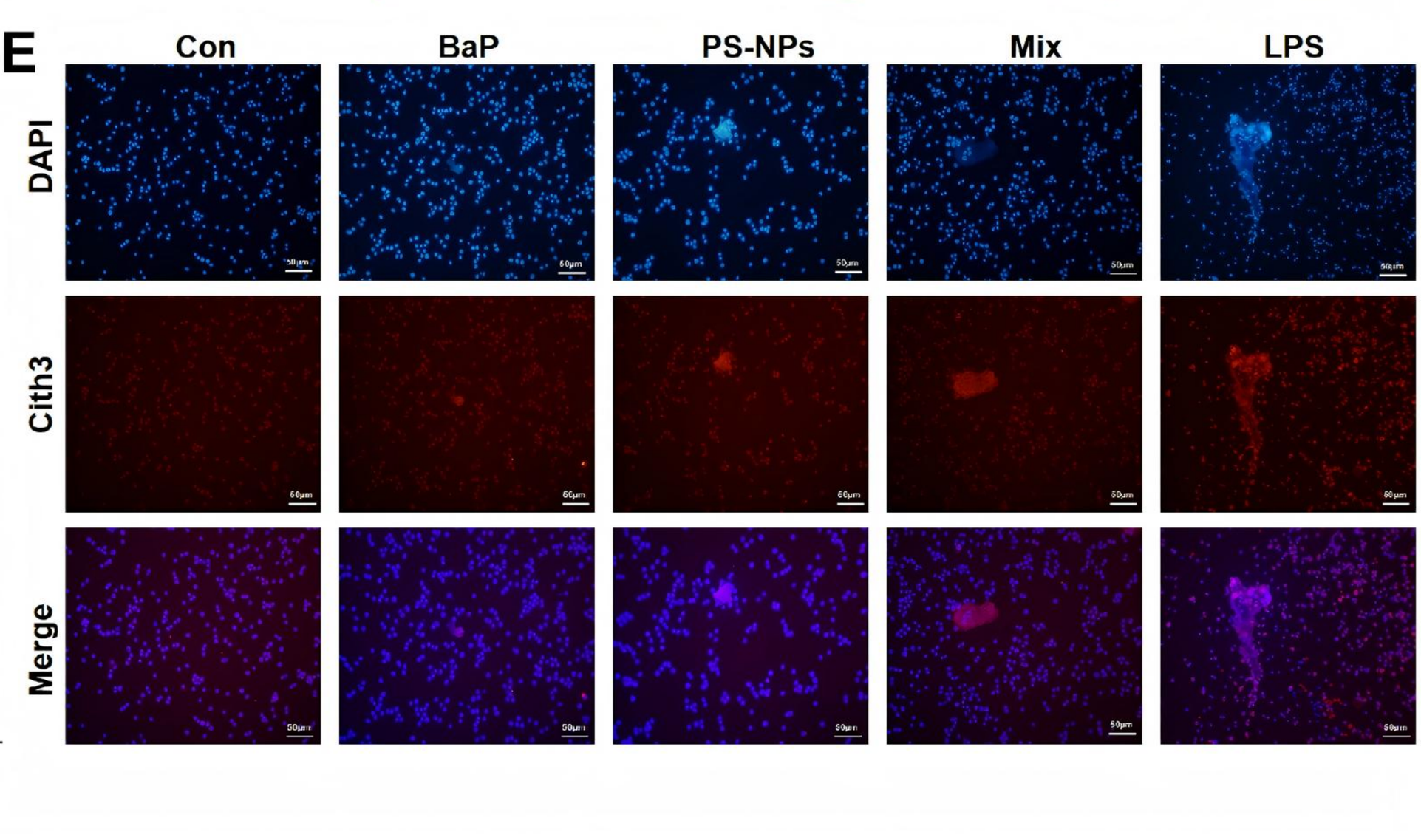
E
Con
BaP
PS-NPs
Mix
LPS
DAPI
Cith3
Merge
50μm

A

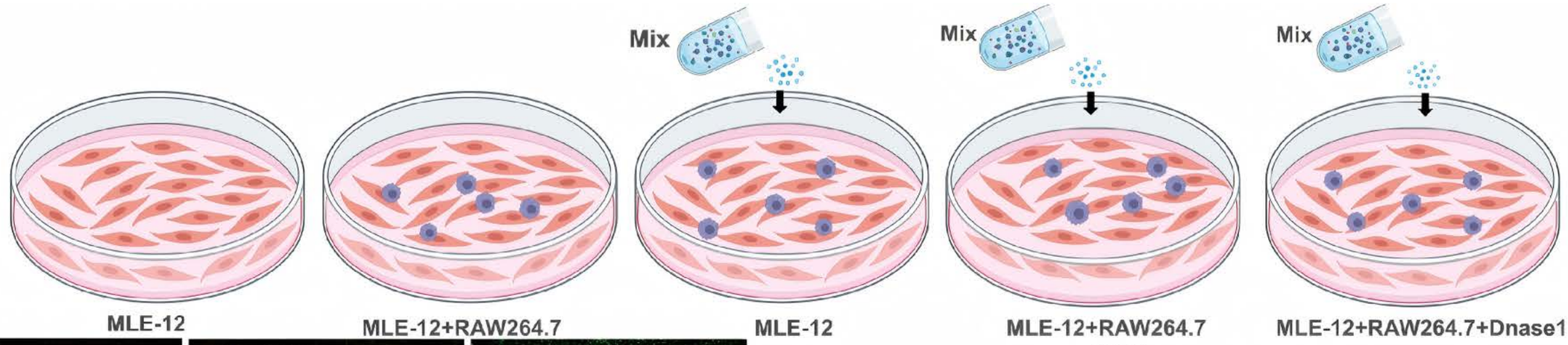
Mix
Mix
Mix
MLE-12
MLE-12+RAW264.7
MLE-12
MLE-12+RAW264.7
MLE-12+RAW264.7+Dnase1

B

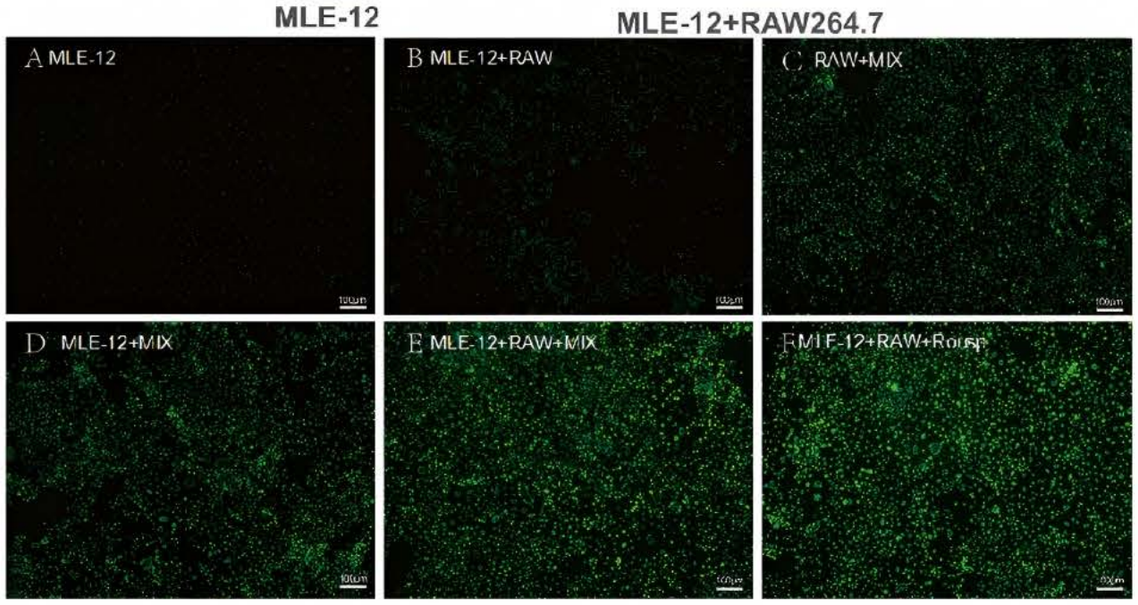
A MLE-12
B MLE-12+RAW
C RAW+MIX
D MLE-12+MIX
E MLE-12+RAW+MIX
F MLE-12+RAW+Rosup

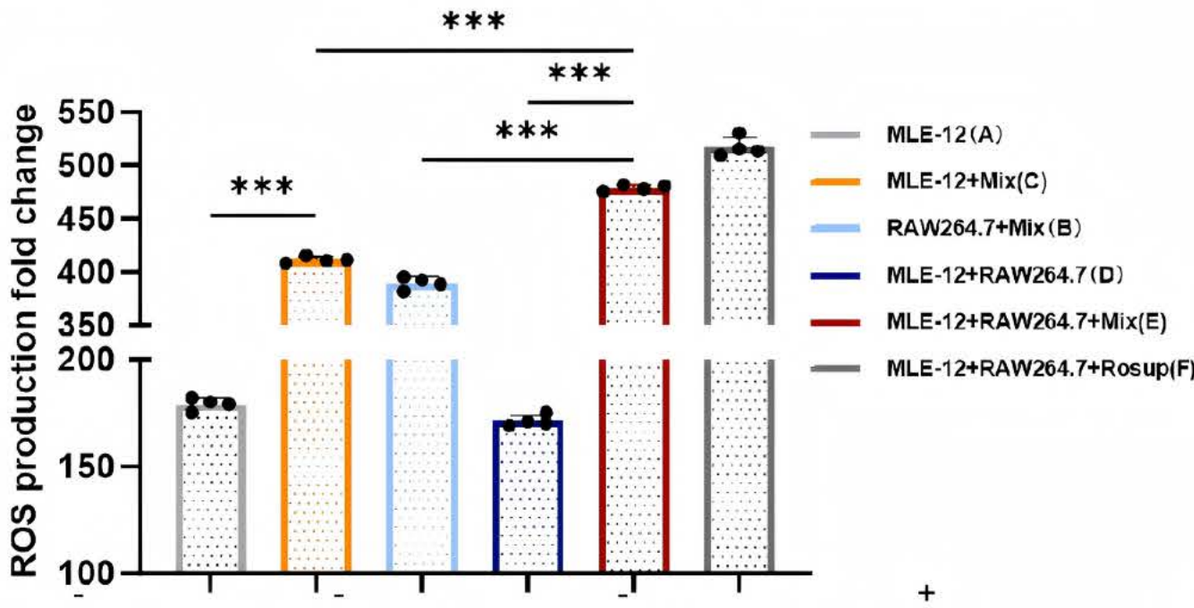
***
***
***
***
ROS production fold change
550
500
450
400
350
200
150
100
MLE-12(A)
MLE-12+Mix(C)
RAW264.7+Mix(B)
MLE-12+RAW264.7(D)
MLE-12+RAW264.7+Mix(E)
MLE-12+RAW264.7+Rosup(F)

C

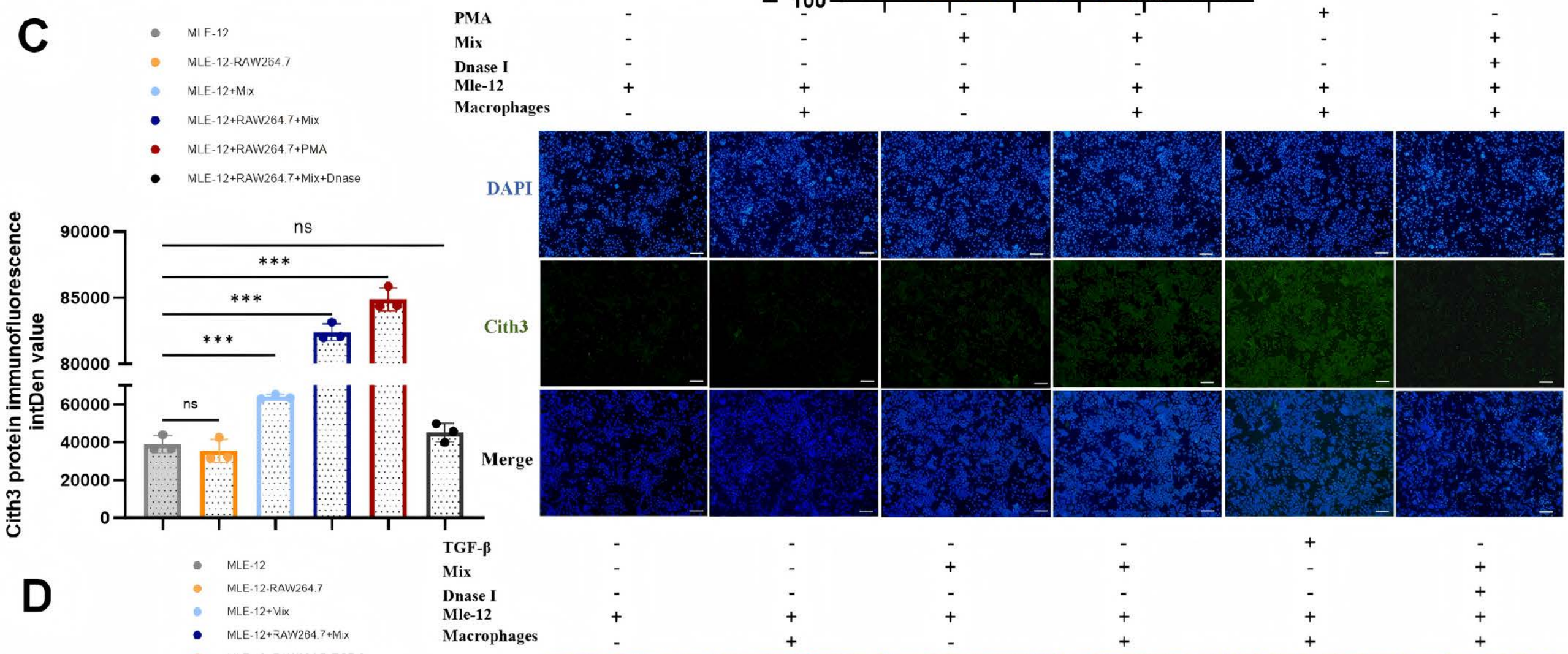
MLE-12
MLE-12-RAW264.7
MLE-12+Mix
MLE-12+RAW264.7+Mix
MLE-12+RAW264.7+PMA
MLE-12+RAW264.7+Mix+Dnase
PMA - - - + -
Mix - - + + - +
Dnase I - - - - - +
Mle-12 + + + + + +
Macrophages - + - + + +
DAPI
Cith3
Merge
Cith3 protein immunofluorescence intDen value
90000
85000
80000
60000
40000
20000
0
ns
***
***
***
ns
TGF-β - - - - + -
Mix - - + + - +
Dnase I - - - - - +
Mle-12 + + + + + +
Macrophages - + - + + +

D

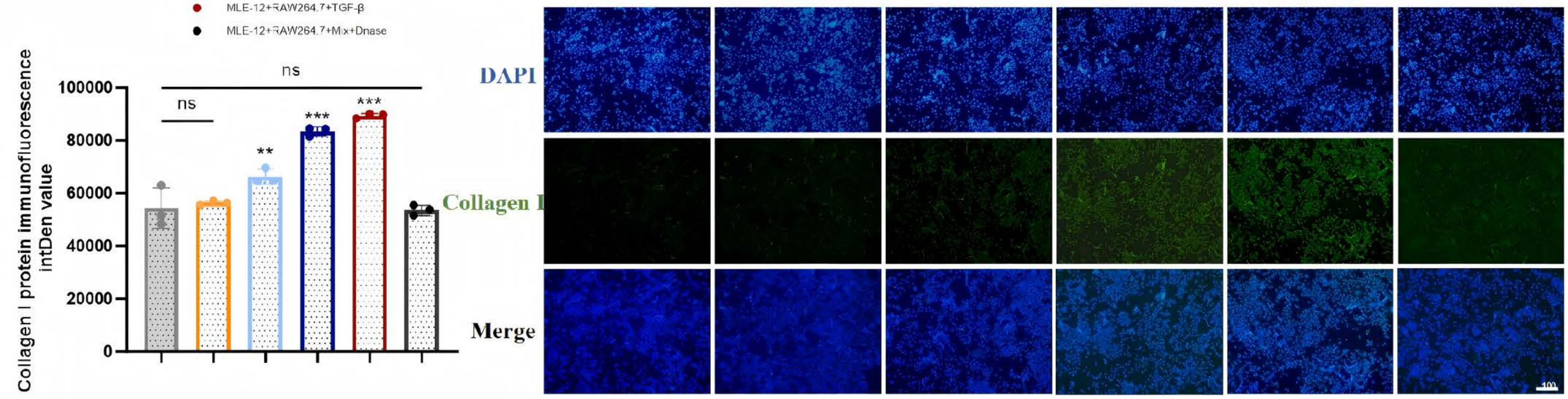
MLE-12
MLE-12-RAW264.7
MLE-12+Mix
MLE-12+RAW264.7+Mix
MLE-12+RAW264.7+TGF-β
MLE-12+RAW264.7+Mix+Dnase
Collagen I protein immunofluorescence intDen value
100000
80000
60000
40000
20000
0
ns
ns
**
***
***
DAPI
Collagen I
Merge

A

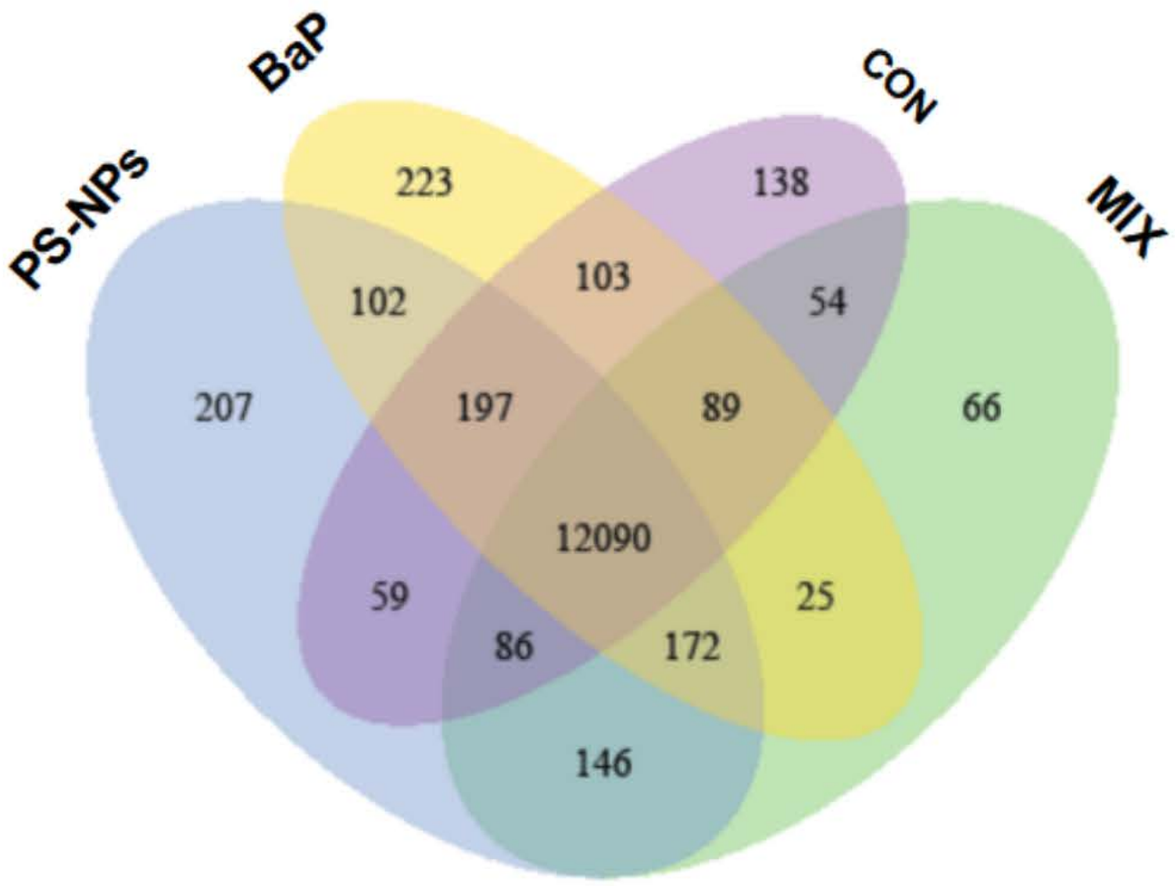
BaP
CON
PS-NPs
MIX
223
138
103
102
54
207
197
89
66
12090
59
25
86
172
146

B

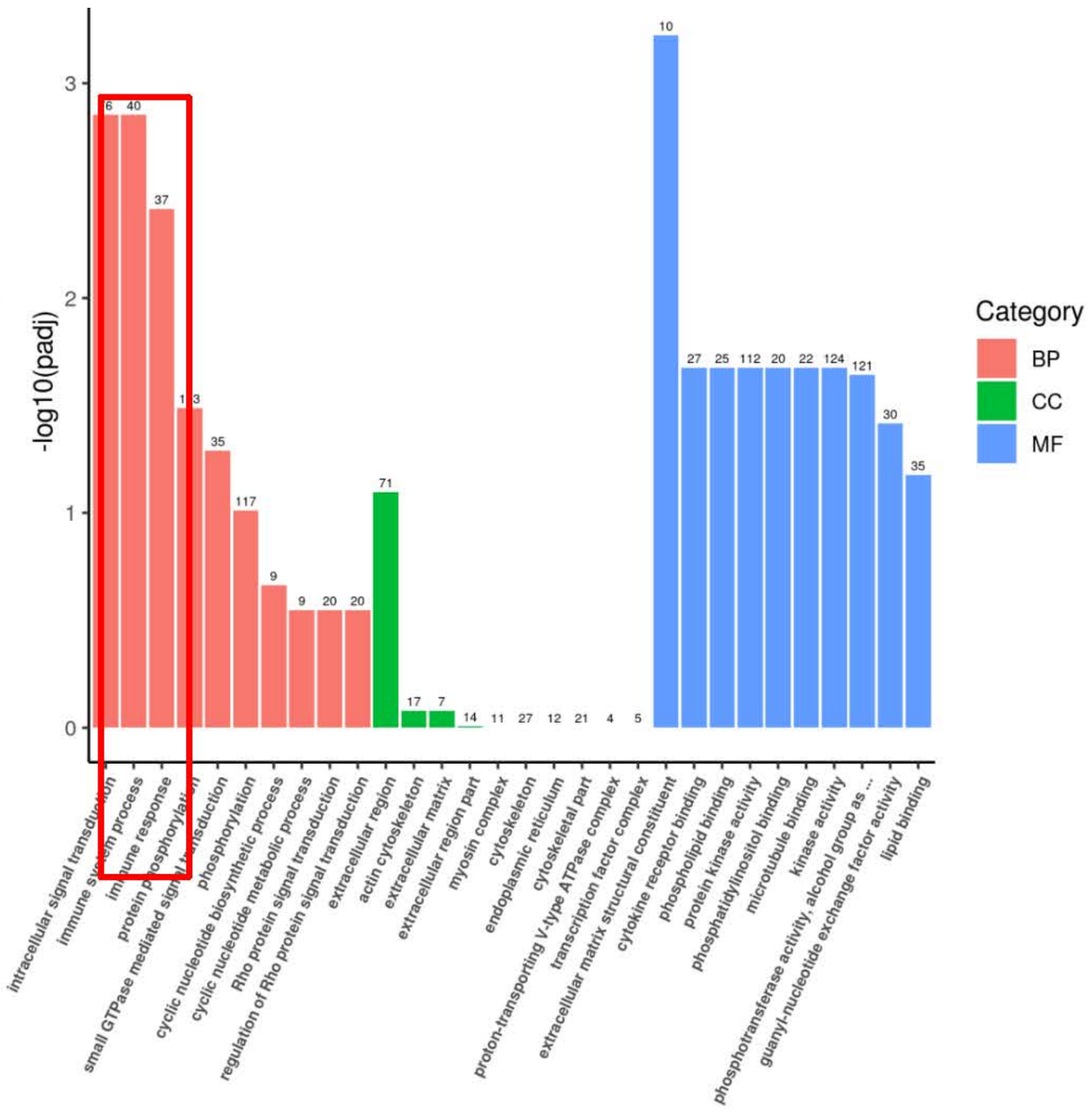
-log10(padj)
Category
BP
CC
MF
intracellular signal transduction
immune system process
immune response
protein phosphorylation
small GTPase mediated signal transduction
phosphorylation
cyclic nucleotide biosynthetic process
cyclic nucleotide metabolic process
Rho protein signal transduction
regulation of Rho protein signal transduction
extracellular region
actin cytoskeleton
extracellular matrix
extracellular region part
myosin complex
cytoskeleton
endoplasmic reticulum
cytoskeletal part
proton-transporting V-type ATPase complex
transcription factor complex
extracellular matrix structural constituent
cytokine receptor binding
phospholipid binding
protein kinase activity
phosphatidylinositol binding
microtubule binding
kinase activity
phosphotransferase activity, alcohol group as ...
guanyl-nucleotide exchange factor activity
lipid binding

C

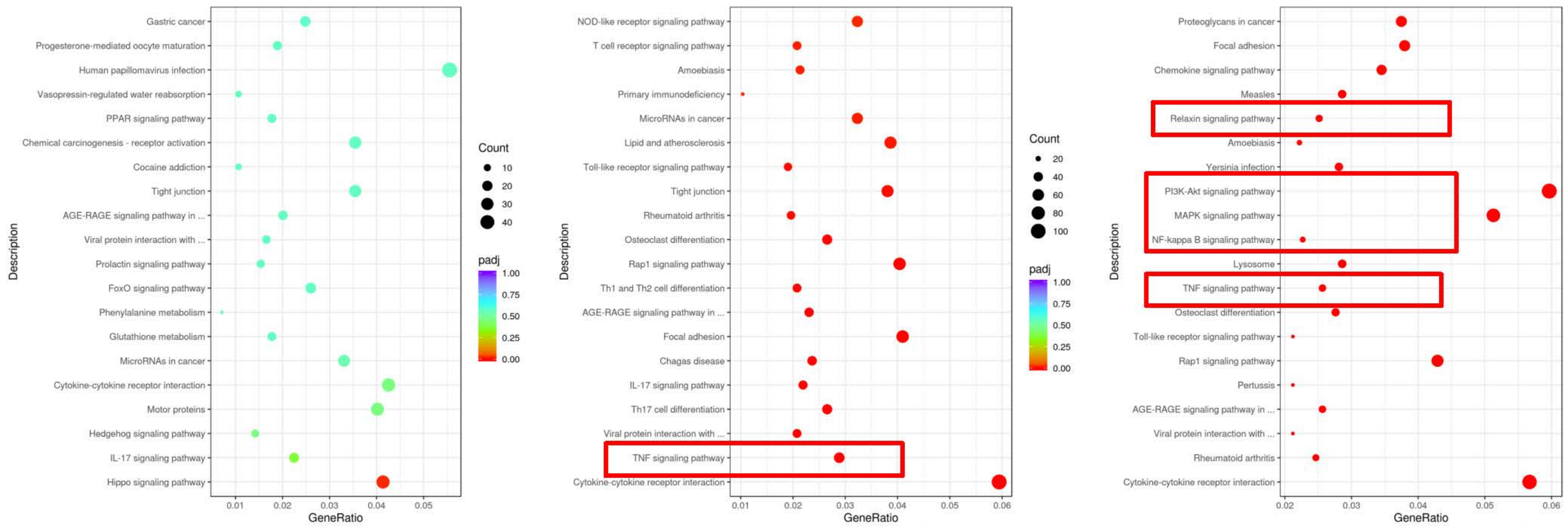
Description
GeneRatio
Count
padj
Gastric cancer
Progesterone-mediated oocyte maturation
Human papillomavirus infection
Vasopressin-regulated water reabsorption
PPAR signaling pathway
Chemical carcinogenesis - receptor activation
Cocaine addiction
Tight junction
AGE-RAGE signaling pathway in ...
Viral protein interaction with ...
Prolactin signaling pathway
FoxO signaling pathway
Phenylalanine metabolism
Glutathione metabolism
MicroRNAs in cancer
Cytokine-cytokine receptor interaction
Motor proteins
Hedgehog signaling pathway
IL-17 signaling pathway
Hippo signaling pathway
NOD-like receptor signaling pathway
T cell receptor signaling pathway
Amoebiasis
Primary immunodeficiency
MicroRNAs in cancer
Lipid and atherosclerosis
Toll-like receptor signaling pathway
Tight junction
Rheumatoid arthritis
Osteoclast differentiation
Rap1 signaling pathway
Th1 and Th2 cell differentiation
AGE-RAGE signaling pathway in ...
Focal adhesion
Chagas disease
IL-17 signaling pathway
Th17 cell differentiation
Viral protein interaction with ...
TNF signaling pathway
Cytokine-cytokine receptor interaction
Proteoglycans in cancer
Focal adhesion
Chemokine signaling pathway
Measles
Relaxin signaling pathway
Amoebiasis
Yersinia infection
PI3K-Akt signaling pathway
MAPK signaling pathway
NF-kappa B signaling pathway
Lysosome
TNF signaling pathway
Osteoclast differentiation
Toll-like receptor signaling pathway
Rap1 signaling pathway
Pertussis
AGE-RAGE signaling pathway in ...
Viral protein interaction with ...
Rheumatoid arthritis
Cytokine-cytokine receptor interaction

D

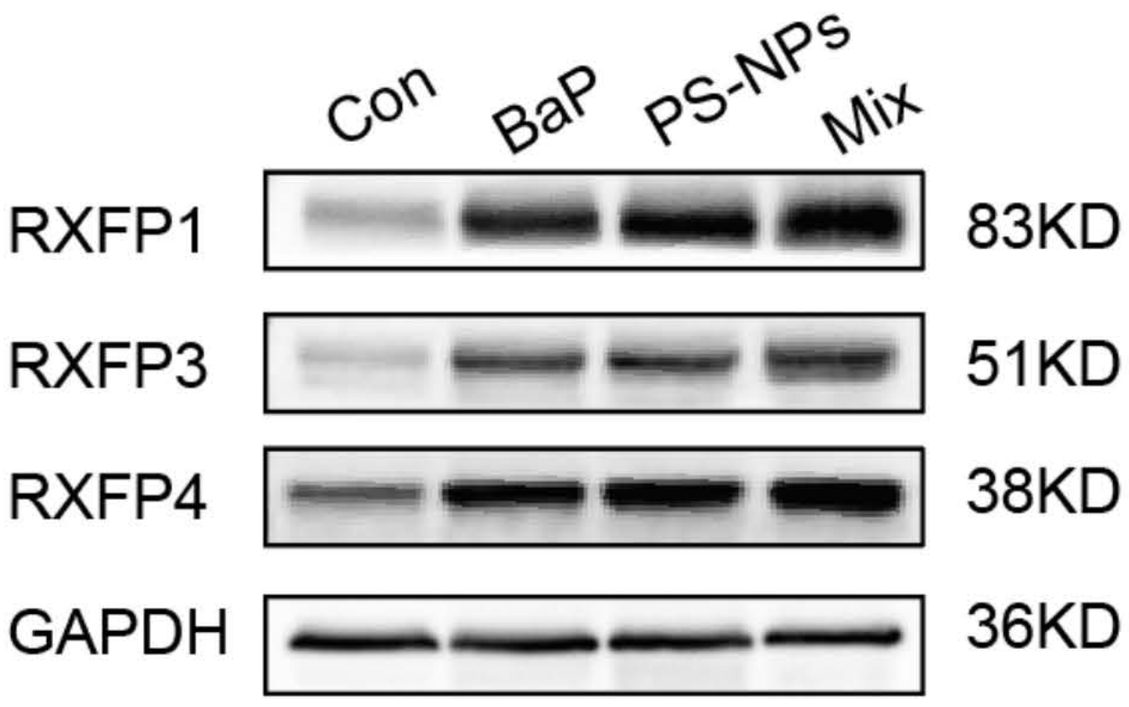
Con
BaP
PS-NPs
Mix
RXFP1
RXFP3
RXFP4
GAPDH
83KD
51KD
38KD
36KD

F

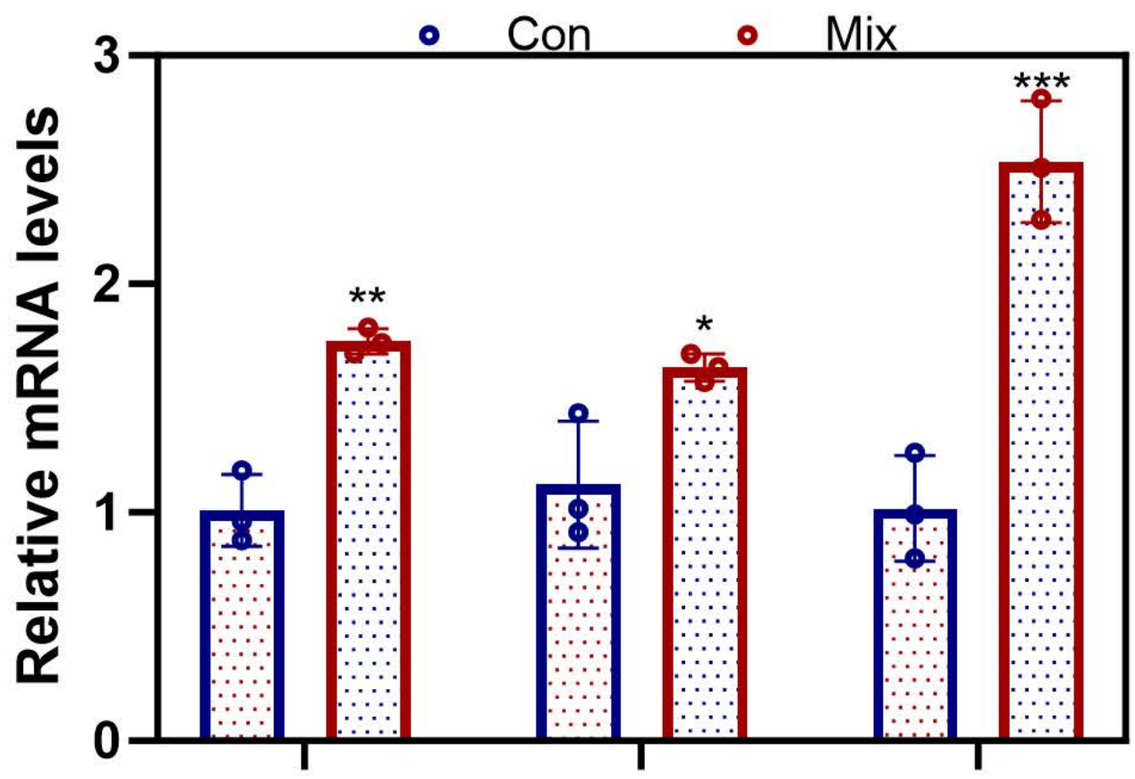
Con
Mix
Relative mRNA levels
RXFP1
RXFP3
RXFP4

E

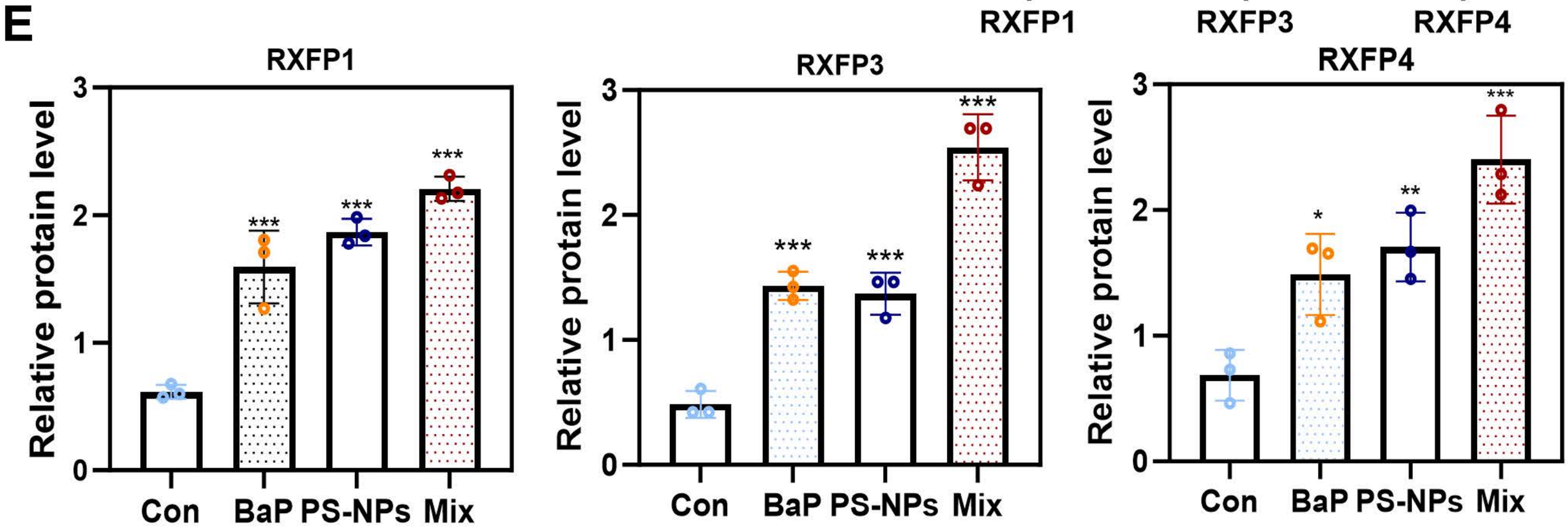
RXFP1
RXFP3
RXFP4
Relative protain level
Con
BaP
PS-NPs
Mix

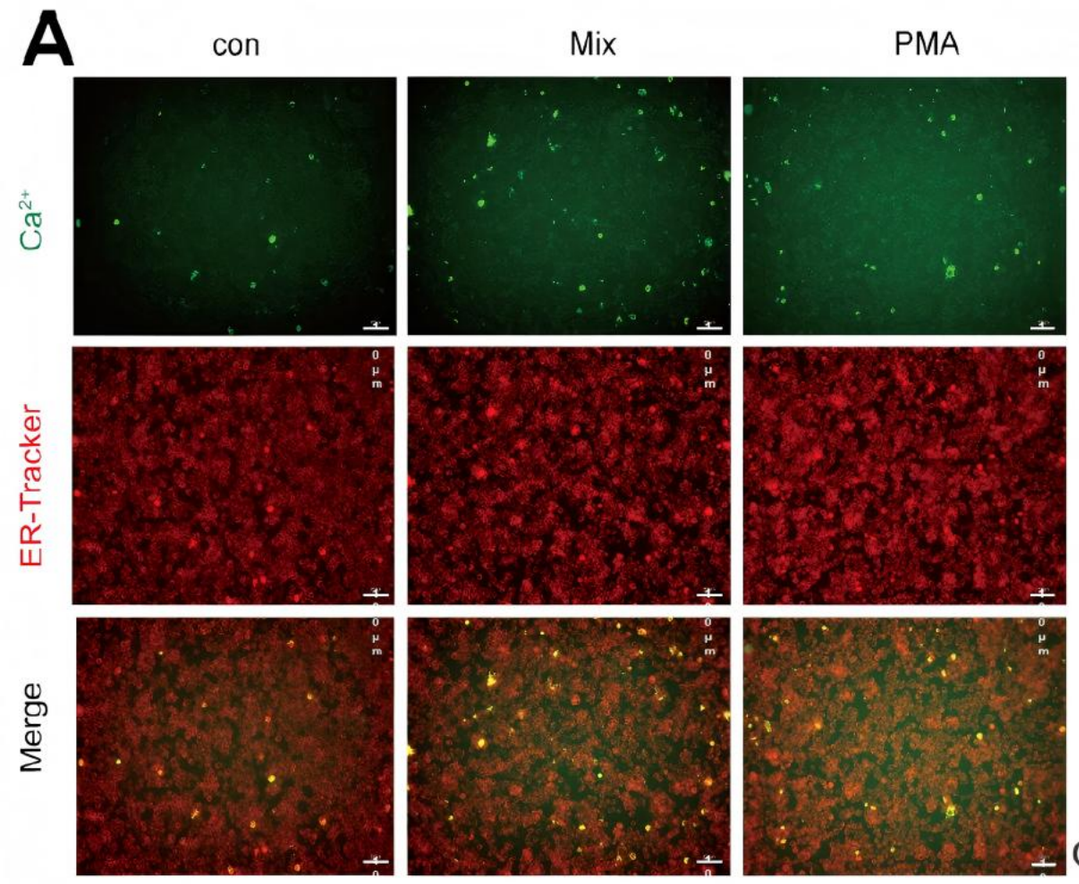
A
con
Mix
PMA
Ca2+
ER-Tracker
Merge

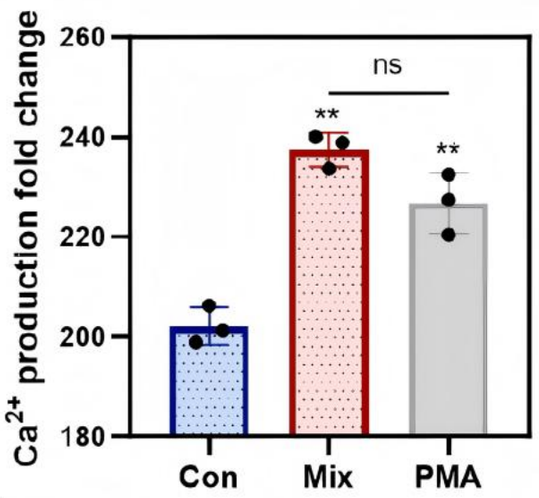
Ca2+ production fold change
260
240
220
200
180
ns
**
**
Con
Mix
PMA

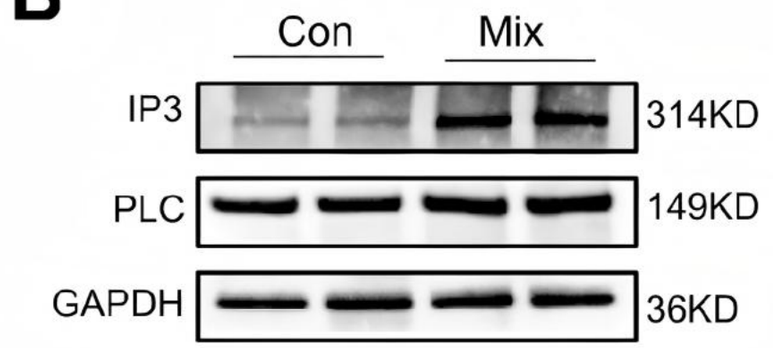
B
Con
Mix
IP3
PLC
GAPDH
314KD
149KD
36KD

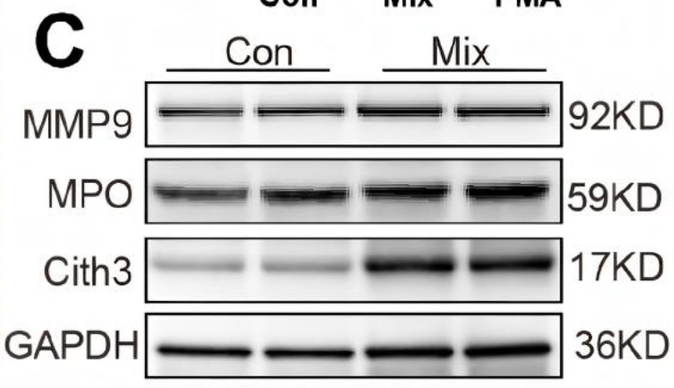
C
Con
Mix
MMP9
MPO
Cith3
GAPDH
92KD
59KD
17KD
36KD

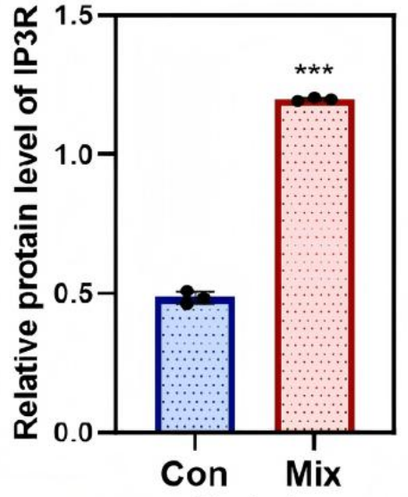
Relative protain level of IP3R
1.5
1.0
0.5
0.0
***
Con
Mix

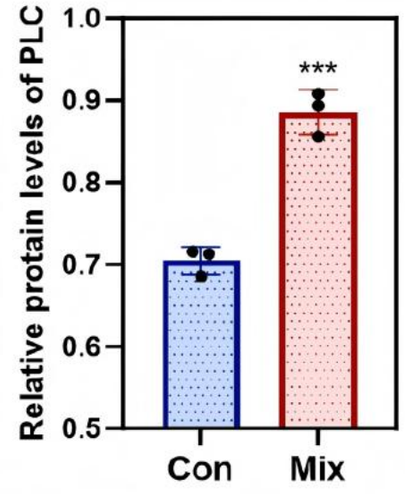
Relative protain levels of PLC
1.0
0.9
0.8
0.7
0.6
0.5
***
Con
Mix

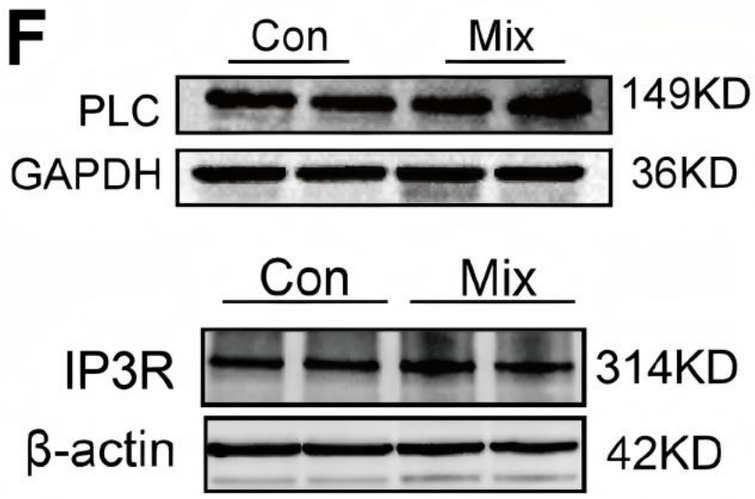
F
Con
Mix
PLC
GAPDH
149KD
36KD
Con
Mix
IP3R
β-actin
314KD
42KD

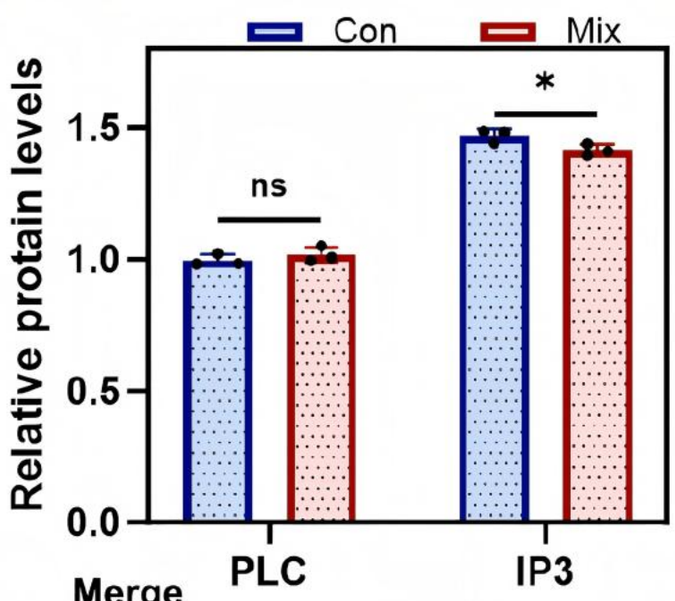
Con
Mix
Relative protain levels
1.5
1.0
0.5
0.0
ns
*
PLC
IP3

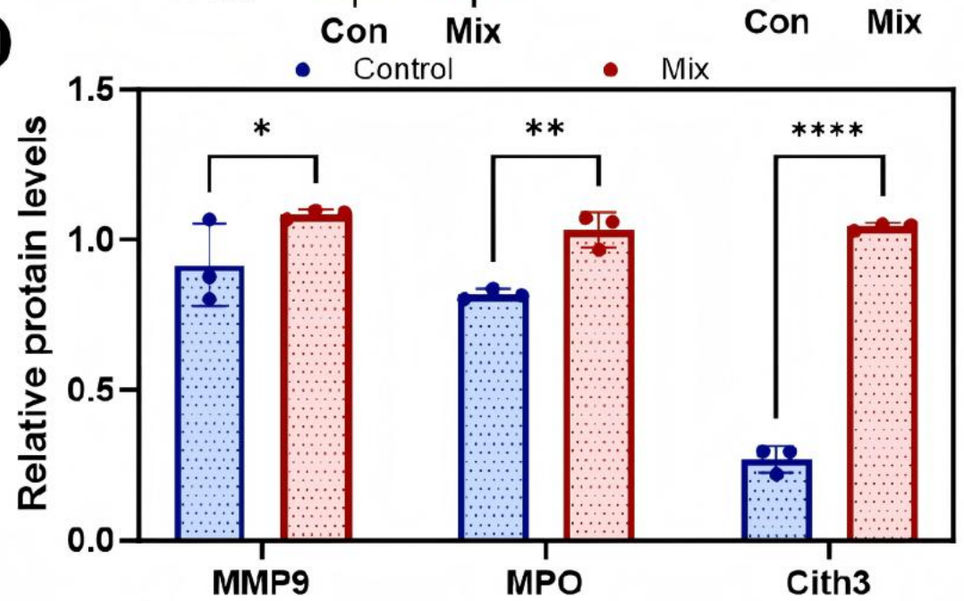
D
Control
Mix
Relative protain levels
1.5
1.0
0.5
0.0
*
**
****
MMP9
MPO
Cith3

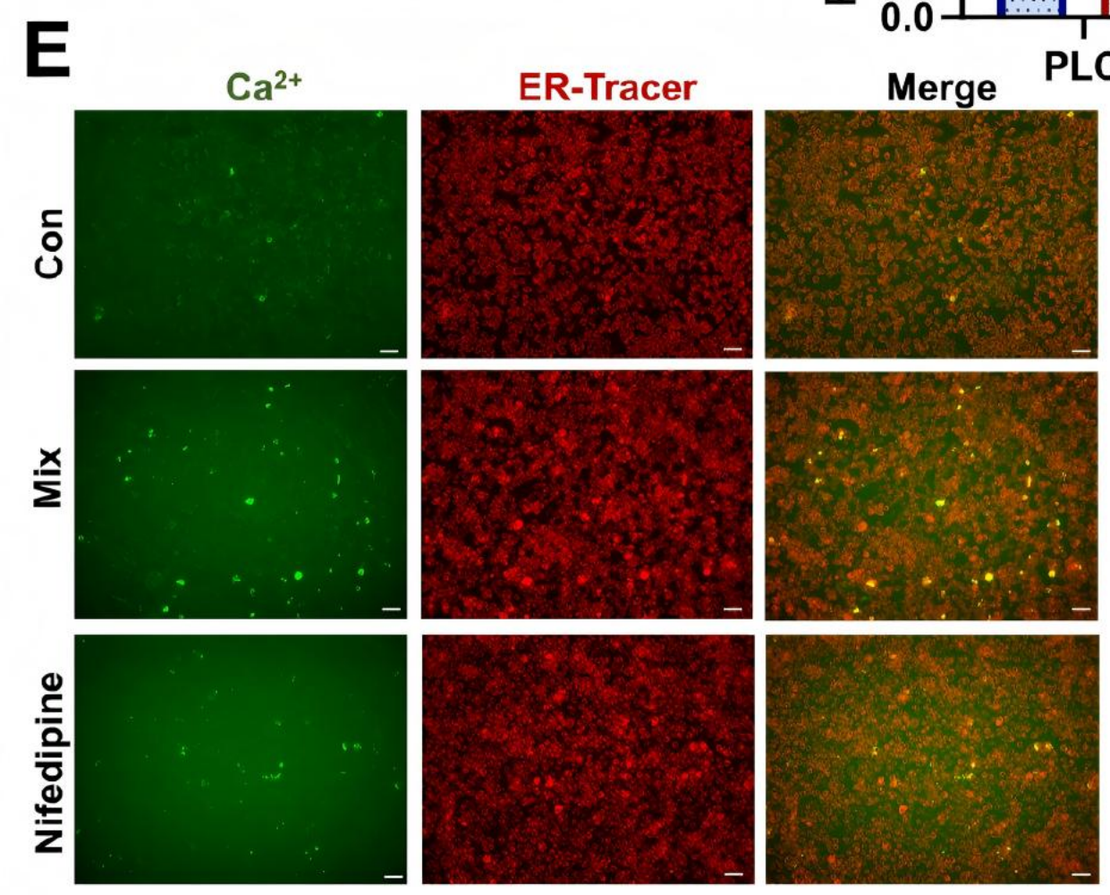
E
Ca2+
ER-Tracer
Merge
Con
Mix
Nifedipine

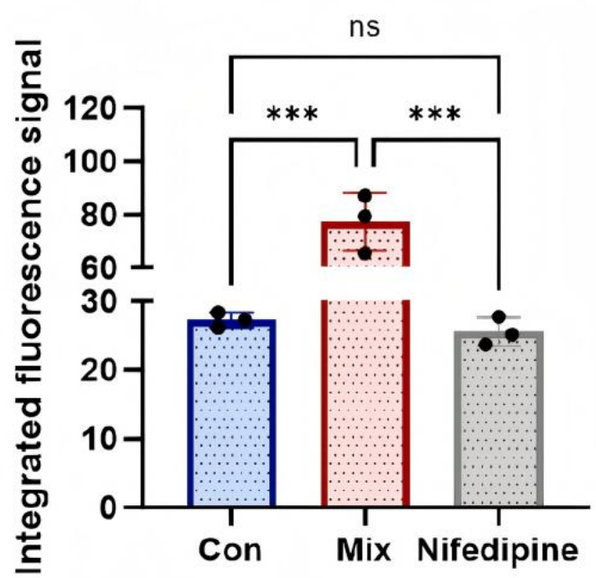
Integrated fluorescence signal
120
100
80
60
30
20
10
0
ns
***
***
Con
Mix
Nifedipine

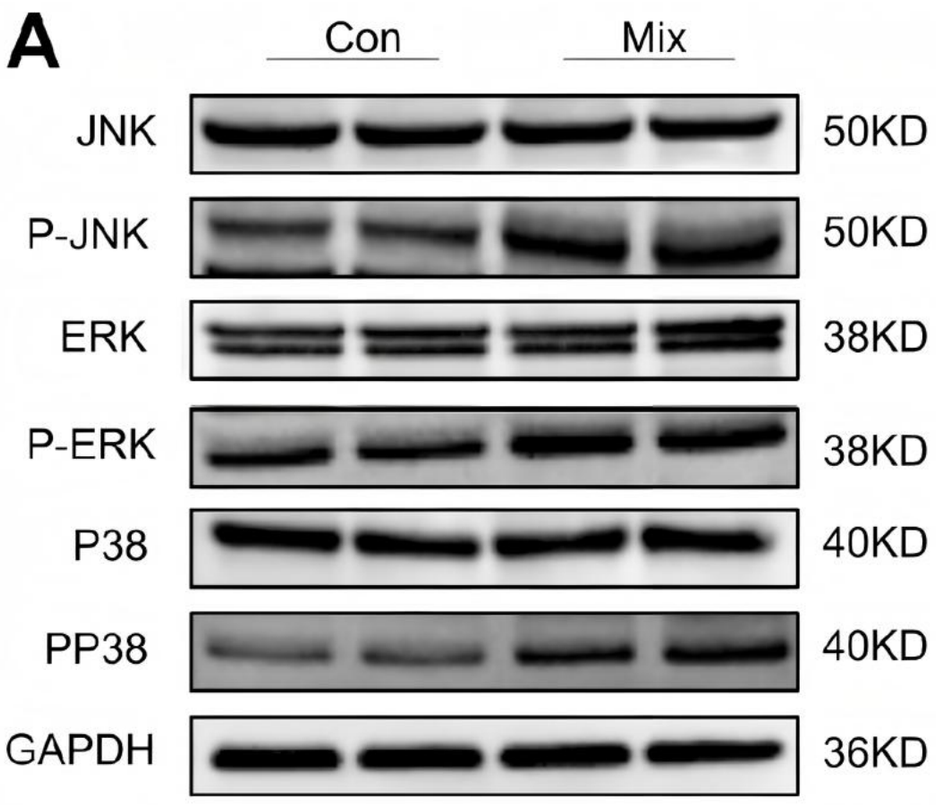
A
Con
Mix
JNK
P-JNK
ERK
P-ERK
P38
PP38
GAPDH
50KD
50KD
38KD
38KD
40KD
40KD
36KD

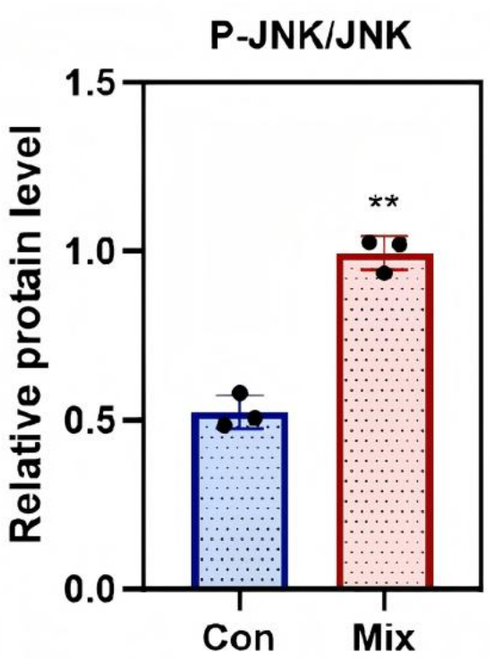
P-JNK/JNK
Relative protain level
1.5
1.0
0.5
0.0
**
Con
Mix

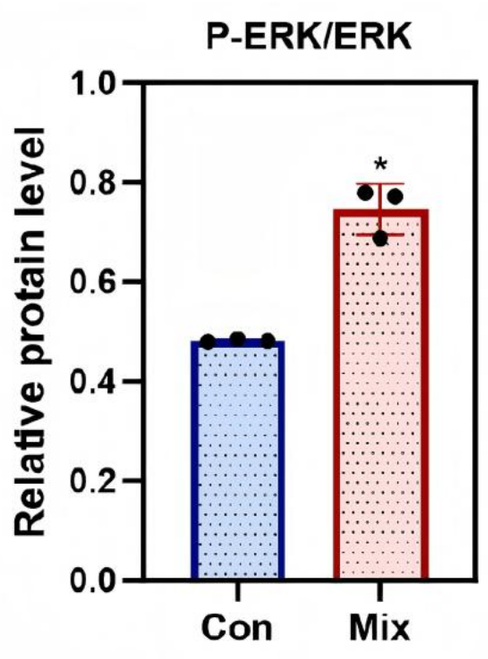
P-ERK/ERK
Relative protain level
1.0
0.8
0.6
0.4
0.2
0.0
*
Con
Mix

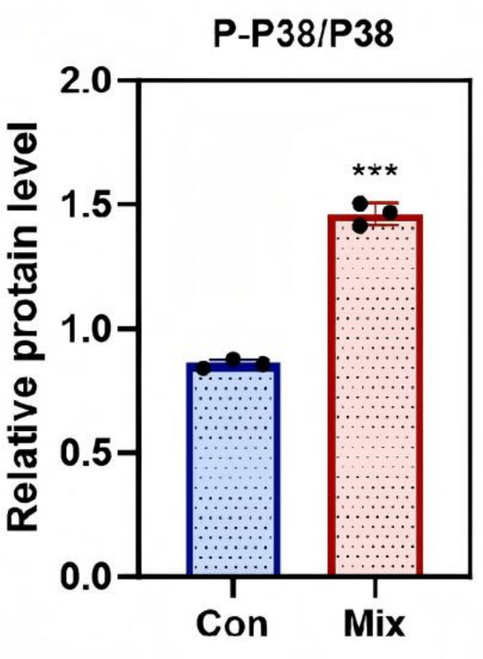
P-P38/P38
Relative protain level
2.0
1.5
1.0
0.5
0.0
***
Con
Mix

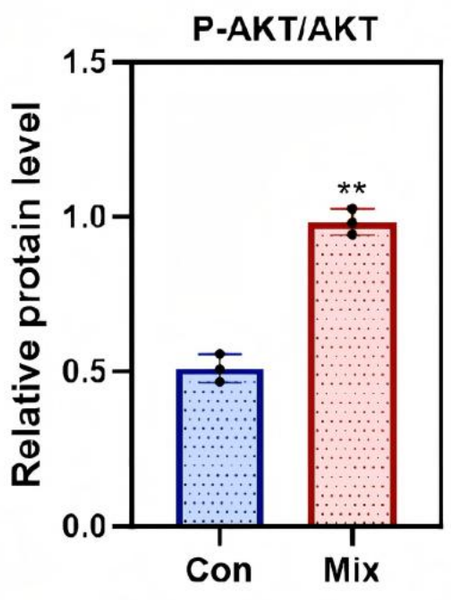
P-AKT/AKT
Relative protain level
1.5
1.0
0.5
0.0
**
Con
Mix

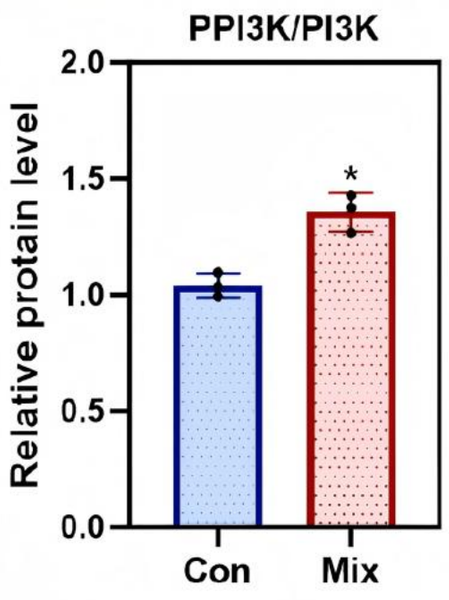
PPI3K/PI3K
Relative protain level
2.0
1.5
1.0
0.5
0.0
*
Con
Mix

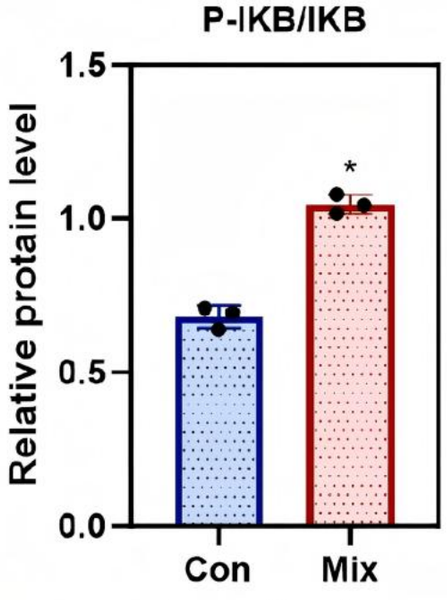
P-IKB/IKB
Relative protain level
1.5
1.0
0.5
0.0
*
Con
Mix

B
Con
Mix
PI3K
PPI3K
AKT
P-AKT
GAPDH
85KD
85KD
56KD
56KD
36KD

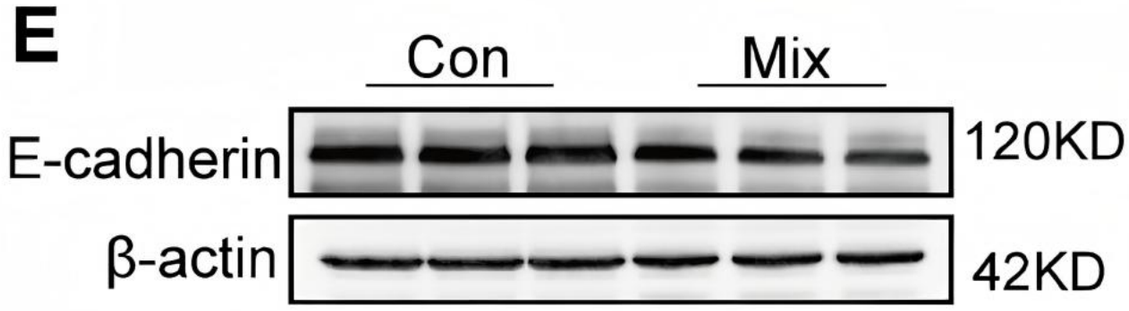
E
Con
Mix
E-cadherin
β-actin
120KD
42KD

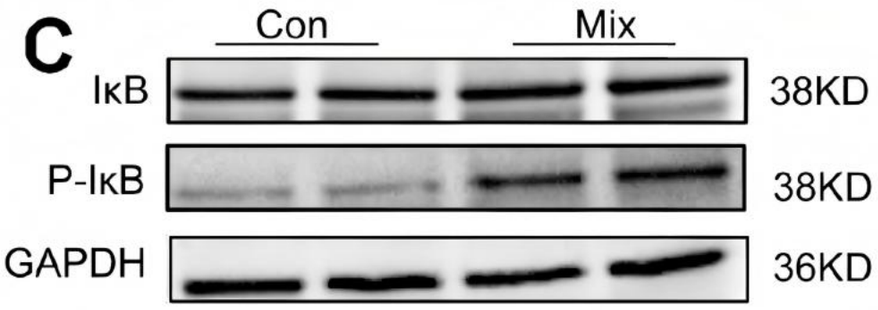
C
Con
Mix
IκB
P-IκB
GAPDH
38KD
38KD
36KD

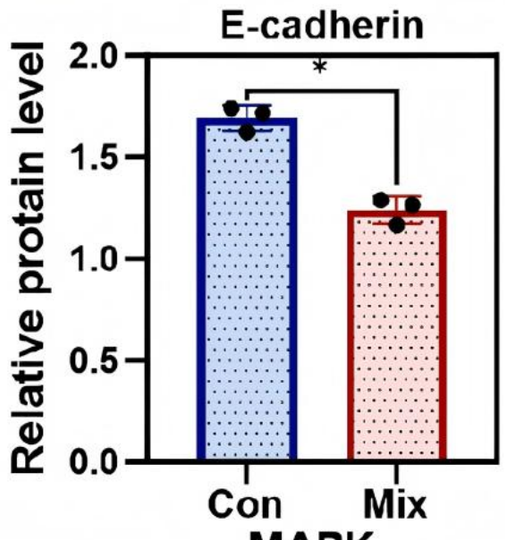
E-cadherin
Relative protain level
2.0
1.5
1.0
0.5
0.0
*
Con
Mix

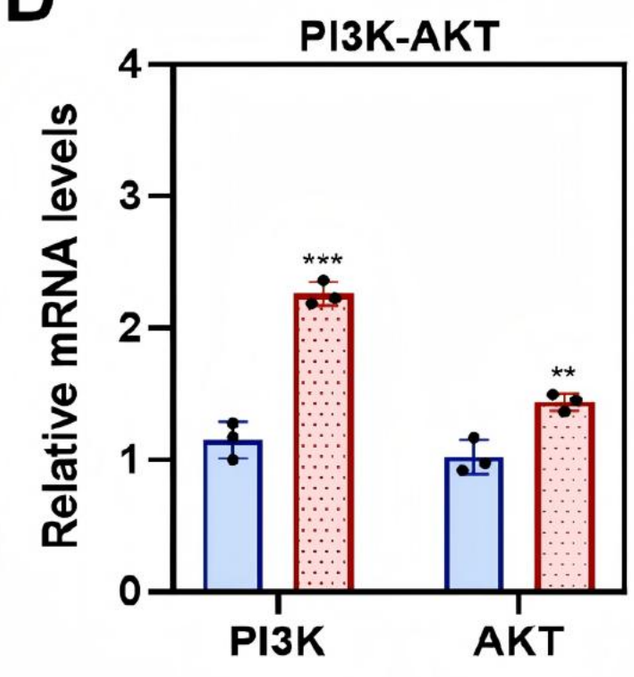
D
PI3K-AKT
Relative mRNA levels
4
3
2
1
0
***
**
PI3K
AKT

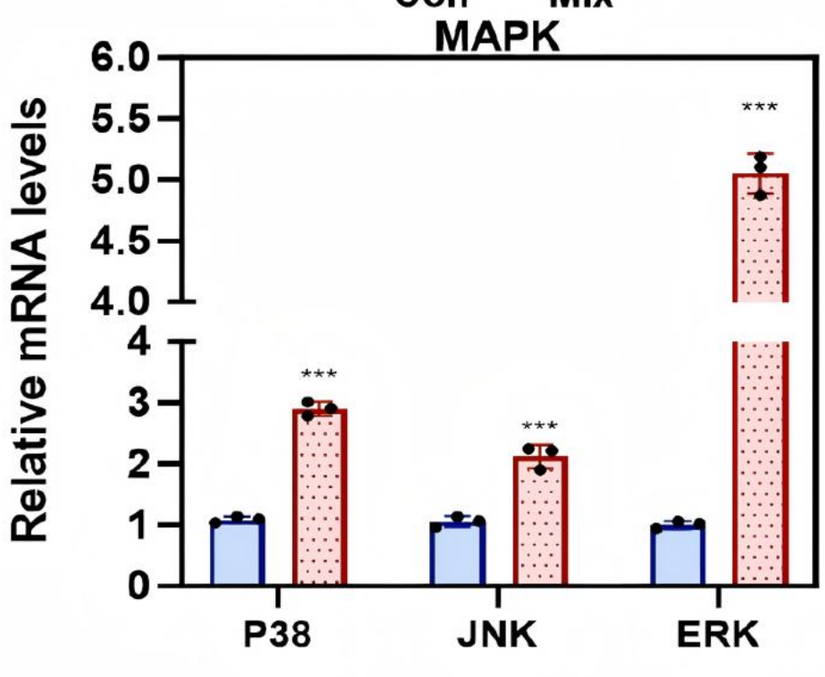
MAPK
Relative mRNA levels
6.0
5.5
5.0
4.5
4.0
4
3
2
1
0
***
***
***
P38
JNK
ERK

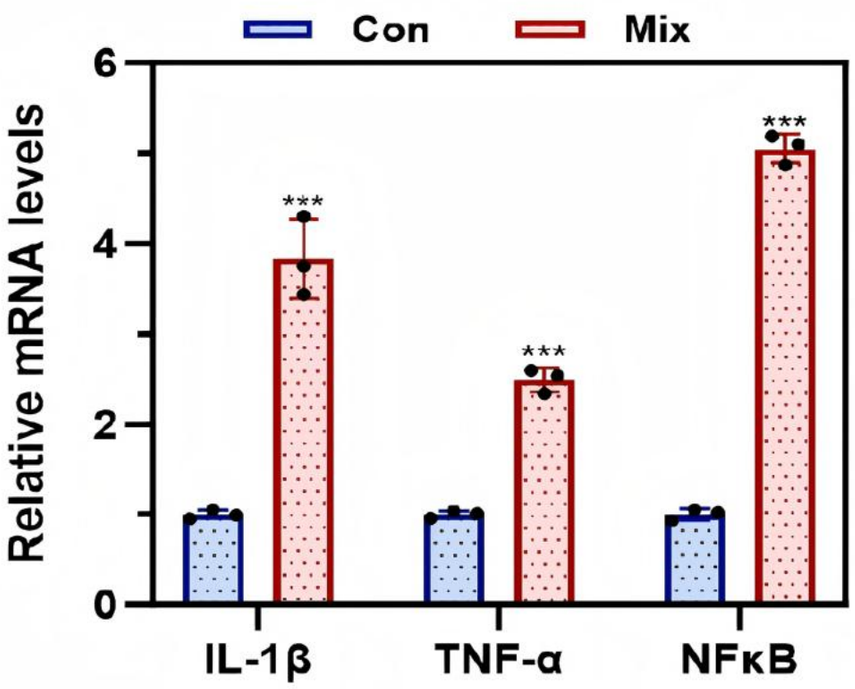
Con
Mix
Relative mRNA levels
6
4
2
0
***
***
***
IL-1β
TNF-α
NFκB

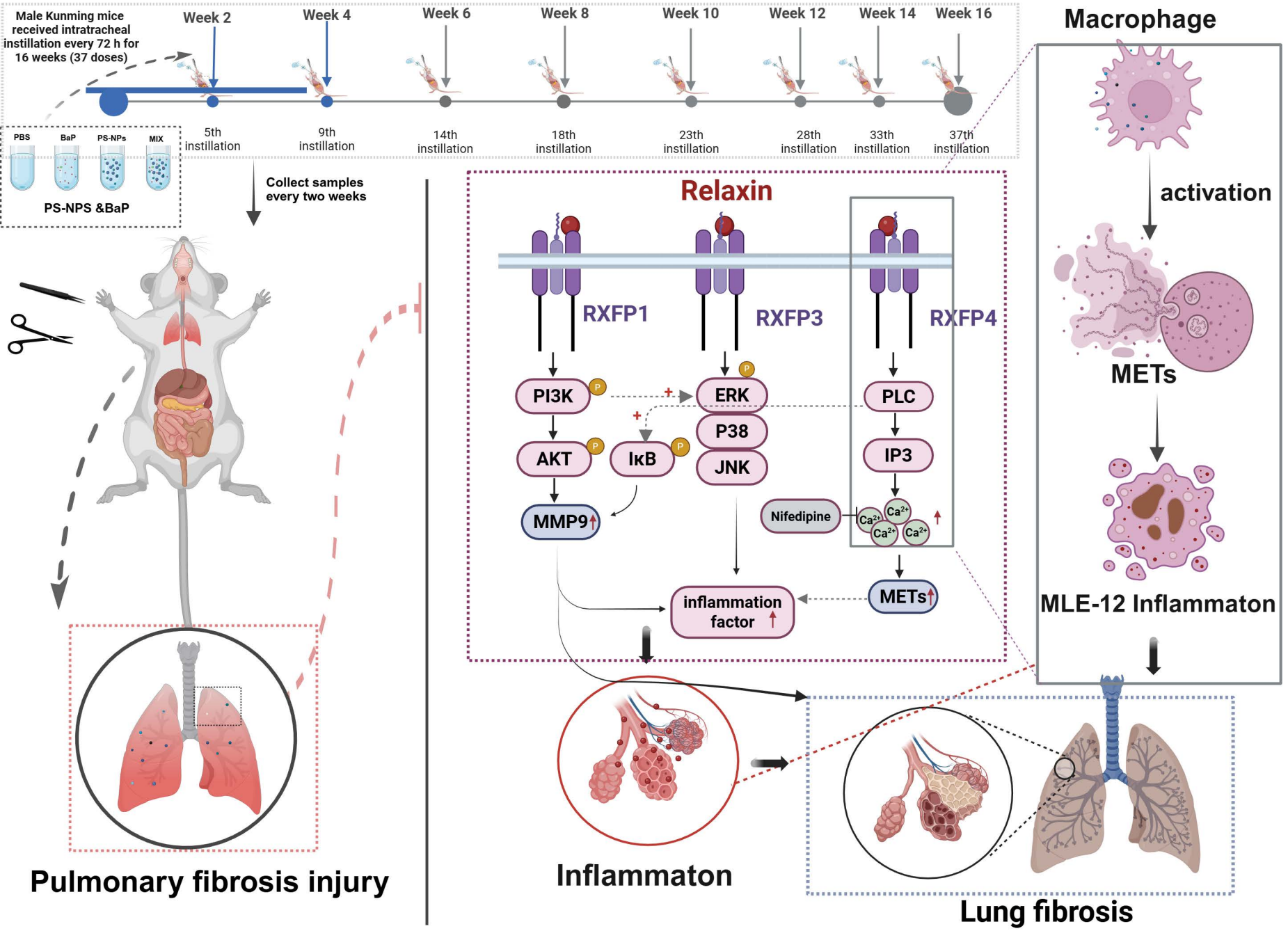
Male Kunming mice received intratracheal instillation every 72 h for 16 weeks (37 doses)
Week 2
Week 4
Week 6
Week 8
Week 10
Week 12
Week 14
Week 16
5th instillation
9th instillation
14th instillation
18th instillation
23th instillation
28th instillation
33th instillation
37th instillation
PBS
BaP
PS-NPs
MIX
PS-NPS &BaP
Collect samples every two weeks
Pulmonary fibrosis injury
Relaxin
RXFP1
RXFP3
RXFP4
PI3K
AKT
MMP9
IκB
ERK
P38
JNK
PLC
IP3
Nifedipine
Ca2+
METs
inflammation factor
Inflammaton
Macrophage
activation
METs
MLE-12 Inflammaton
Lung fibrosis